MiR-146a-dependent regulation of CD24/AKT/β-catenin axis drives stem cell phenotype in oral cancer

Sangeeta Ghuwalewala[1a*], Dishari Ghatak[1b*], Sumit Das[2c], Pijush Das[1d], Ramesh Butti[2e] Mahadeo Gorain[2f], Gopal C Kundu[2g]and Susanta Roychoudhury[1,3#]

[1]Cancer Biology and Inflammatory Disorder Division, CSIR-Indian Institute of Chemical Biology,4, Raja S.C. Mullick Road, Jadavpur, Kolkata-700032, India.

[a]sangeetaghuwalewala@gmail.com,[b]dishari18@gmail.com,[c]das.sumit13@gmail.com, [d]topijush@gmail.com, [e]rameshbutti@gmail.com, [f]mahadeo.gorain@gmail.com, [g]kundu@nccs.res.in

[2]Laboratory of Tumor Biology, Angiogenesis and Nanomedicine Research, National Centre for Cell Science (NCCS), Pune 411007, India.

[3]Division of Research, Saroj Gupta Cancer Centre and Research Institute, Mahatma Gandhi Road, Thakurpukur, Kolkata 700063, India

#To whom correspondence should be addressed

Susanta Roychoudhury, PhD, Saroj Gupta Cancer Centre and Research Institute, Mahatma Gandhi Road, Thakurpukur, Kolkata 700063, India, E-mail: susantarc@gmail.com

[*]These authors contributed equally to this work.

Running title: MiR-146a regulate CSCs by targeting CD24

Abstract

Cancer stem cells (CSCs) are known to potentiate tumor initiation and maintenance in oral squamous cell carcinoma (OSCC). Increasing evidences suggest that $CD44^{high}CD24^{low}$ population in OSCC exhibit CSC-like characteristics. The role of mi-RNAs in maintenance of oral CSCs has remained unclear. Here we report that $CD44^{high}CD24^{low}$ population within OSCC cell lines and primary HNSCC

tumors have an elevated expression of miR-146a. Moreover, over-expression of miR-146a results in enhanced stemness phenotype by augmenting $CD44^{high}CD24^{low}$ population. We demonstrate that miR-146a induces CSC property by stabilizing β-catenin with concomitant loss of E-cadherin and CD24. Interestingly, CD24 has been identified as a novel functional target of miR-146a and ectopic expression of CD24 abrogates miR-146a driven potential CSC phenotype. Mechanistic analysis reveals that higher CD24 levels inhibit AKT phosphorylation leading to β-catenin degradation in non-CSCs. We also validate that the miR-146a/CD24/AKT loop significantly alters tumorigenic ability *in vivo*. Furthermore, we confirmed that β-catenin trans-activates miR-146a, thereby forming a positive feedback loop contributing to stem cell maintenance. Collectively, our study demonstrates that miR-146a regulates CSC-driven properties in OSCC through CD24-AKT-β-catenin axis.

Keywords: miR-146a, β-catenin, AKT, stemness, CD24, OSCC

Introduction

Oral Squamous Cell Carcinoma (OSCC) is the most prevalent form of head and neck cancers worldwide with more than 60% individuals diagnosed with advanced tumors[1]. It is known that cancer stem-like cells (CSC) leads to aggressive tumor behavior [2]. The oral tumor CSCs are also considered responsible for treatment failures, relapse and development of metastases [3,4]. Over the past decade, epigenetic re-programming has emerged as a crucial mechanism of regulating cancer stem cell dynamics [5]. Epigenetic regulatory mechanisms include DNA methylation, histone modifications and chromatin remodeling. They show robust effect upon cellular fate and stem cell potential [6,7]. MiRNAs, a small ncRNAs of 20-22 nucleotides, has recently gained considerable importance in epigenetic modulation of tumor [8]. De-regulation of miRNAs may have critical roles in disease development [9].They can act either as oncogenes or as tumor-suppressors depending upon the specific genes targeted. In-fact miRNA associated signatures are now considered for cancer specific diagnostic and prognostic purposes [10].

MiRNAs not only regulate primary cellular functions like proliferation, differentiation, migration and invasion, but are also directly or indirectly involved in CSC functions [11-14]. Most of this phenomenon are attributed to altered signaling pathways including cell surface markers, pluripotent transcription factors, chemo-resistance and epithelial-to-mesenchymal transition (EMT) markers[15].Role of miR-34a, miR-145a and miR-200bc family in regulating CD44, Oct4, Sox2, KLF4, Bmi1, Zeb1/2 and Notch1 has been well established[16-19]. Thus, by precisely regulating the CSC related genes, miRNAs themselves have emerged as inherent modulators of cancer stem cells.MiR-146a is predominantly an onco-miR, which directly targets *IRAK1*, *traf6*, and *numb* genes in OSCC and imparts tumorigenicity [20].Emerging evidence on miR-146a suggests that it directs the self-renewal process in colorectal cancer stem cells by regulating Snail-β-catenin axis which also contributes to EMT[21].High nuclear accumulation of β-catenin, along with lowering of E-cadherin is frequently associated with higher tumor grade and poor prognosis in various cancers[22]. Given the role of Wnt/β-catenin signaling in CSC maintenance and the miRNAs in regulating wnt pathway, understanding the step-wise regulation of its mediators is crucial [23-25].

Our recent study has characterized $CD44^{high}CD24^{low}$ cells as the potential CSC population in OSCC[3]. CD24, a small cell surface protein, was identified as a critical determinant of differentiation in hematopoietic cells and mammary epithelial cells[26]. Besides having role in adhesion, cadherin switching or migration, CD24 is involved in diverse signaling networks, thus promoting oncogenesis or regression[27]. Although role of CD44 is well established[4], the significance of CD24 in determining stemness is less explored, particularly in oral CSCs. In this study, we show that miR-146a imparts $CD44^{high}CD24^{low}$status to OSCC cells merely by targeting CD24. Changes in β-catenin pools seemed to be an important event in altering the afore-mentioned phenotypes downstream of miR-146a through AKT pathway. We propose that miR-146a/CD24/AKT/β-catenin axis influences the stemness characteristics of $CD44^{high}CD24^{low}$ population in oral cancer cells.

Results

MiR-146a is over-expressed in $CD44^{high}CD24^{low}$ population of OSCC cell lines and primary tumors

To identify the cellular miRNAs regulating CSC phenotype of OSCC cells, we initially screened nine miRNAs that are aberrantly expressed in human cancers with their reported role in cancer stemness and EMT [30-32]. QRT-PCR data showed significant difference in the expression of miR-200b, miR-138, miR-34a, miR-21 and miR-146a between$CD44^{high}CD24^{low}$ and $CD44^{low}CD24^{high}$ population of SCC25 cells (Fig. 1a). Amongst them, we focused on miR-146a in view of its context dependent role in various cancers[33-35].MiR-146a is consistently over-expressed in oral CSCs, therefore it was intriguing to explore its possible connection with stemness and the underlying mechanisms. Up-regulation of miR-146a in the $CD44^{high}CD24^{low}$ population of SCC131 and SCC084 cell lines was also confirmed (Fig.1b). Further, miR-146a expression was also increased upon enrichment of isolated CSCs in the sphere forming culture conditions, suggesting its importance in determining oral CSC property (Fig. 1c). Increased miR-146a expression has been reported to predict poor survival of OSCC patients[20]. Our analyses in TCGA Head and Neck Squamous cell Carcinoma (HNSCC) patient's cohort[36], showed increased miR-146a expression in patients with $CD44^{high}CD24^{low}$signature compared to those with $CD44^{low}CD24^{high}$profile (Fig. 1d). While there was not much difference in the histological stage of the tumors across the two categories, most of the $CD44^{low}CD24^{high}$ tumors were free of lymph node metastasis (Figure S1a, Supplementary file 1). Moreover, miR-146a expression of the node positive patients was relatively higher than that of the node negative ones, although not statistically significant (Figure S1b). Together, our data suggests high miR-146a expression as a critical determinant of CSC phenotype in oral tumors.

Ectopic expression of miR-146a induces CSC characteristics

We next investigated whether ectopic miR-146a affect CSC markers and found a significant increase in the relative proportion of$CD44^{high}CD24^{low}$ population in SCC131 cells (Fig.2a). Similar results were also obtained with SCC036, SCC084 and SCC25 cells, respectively (Figure S2a). Characteristic sphere forming ability of miR-146a expressing SCC131 and SCC036 cells were also markedly enhanced (Fig.

2b). Concomitantly, ectopic expression of miR-146a led to the increased expression of intracellular stem cell markers such as Oct4, Sox2 and C-myc and loss of Involucrin (Fig.2c). Also, we observed a pronounced decrease in CD24 protein levels upon ectopic miR-146a expression in SCC036, SCC131 and SCC084 cells (Fig. 2c). However, in SCC131 cells the levels of Oct4 and Involucrin did not show a dose dependent change upon miR-146a over-expression, probably due to high endogenous miR-146a in this cell line (Fig. 2c and Figure S2b). Loss of these markers upon knockdown of miR-146a was also evident in SCC131 and SCC25 cells (Figure S2c). Expression of miR-146a transcripts was validated by qRT-PCR (Figure S2d). Transfection of miR-146a containing mutated seed sequence, however, did not alter the levels of stem-related proteins in a statistically significant manner (Fig. 2d).These results demonstrate that miR-146a contributes to enrichment of CSCs in OSCC through increased expression of stem cell markers.

MiR-146a activates Wnt/β-catenin pathway and promotes EMT in oral CSCs

The CSC population is sustained by niche signalling, similar to that of normal stem cells. These include Wnt, Notch and Hedgehog pathways that are often involved in maintaining its self-renewal potential [37]. Accordingly, we observed increased expression of β-catenin and Cleaved Notch1 in $CD44^{high}CD24^{low}$ population of SCC25 and SCC131 cells (Figure S3a, b).While significantly depleted in $CD24^{high}$cells, β-catenin levels were also higher in $CD24^{low}$ population of SCC084 cells which correlated well with the expression of stemness markers in these cells (Fig.3a). To specifically envisage the role of CD24, we now compared the $CD44^{high}CD24^{low}$ population with the $CD44^{high}CD24^{high}$ cells only. Interestingly we detected nuclear localization of β-catenin in the $CD44^{high}CD24^{low}$ population of SCC131 cells,whereas it remained membrane bound in $CD44^{high}CD24^{high}$cells(Fig.3b). Transcriptional activity of β-catenin was indicated by the relative wnt reporter activity in the respective cell populations (Figure S3c). Interestingly, upon stable knockdown of β-catenin, not only the stem cell markers were reduced but also a modest increase in CD24 expression was observed (Figure S3d). These results suggest a possible cross talk between CD24 and β-catenin in conferring stemness and EMT to these cells.

The clue that β-catenin level might influence stemness in OSCC cells led us to investigate whether miR-146a regulates β-catenin. Indeed, over-expression of miR-146a lead to the dose dependent increment in β-catenin levels with concordant decrease in E-cadherin (Fig.3c). It is known that miR-146a targets the 3'UTR of Numb, a protein that promotes lysosomal degradation of β-catenin and Cleaved Notch1 [38].We indeed, confirmed reduced levels of Numb upon miR-146a over-expression along with stabilization of Cleaved Notch1(Figure S3e). Conversely, inhibition of miR-146a activity lead to β-catenin degradation along with the loss of Oct4 as expected (Fig.3d). Notably, we did not observe these changes upon mutant miR-146a over-expression (Figure S3f). To emphasize the contribution of β-catenin in miR-146a induced stemness, we transfected miR-146a in β-catenin shRNA expressing cells and found no change in expression of CSC markers (Figure S3g) as compared to that of non-silencing controls. Strikingly, the ability of anchorage independent growth induced by miR-146a was also dependent on the expression of β-catenin (Figure S3h) suggesting its tumorigenic role in OSCC.

To obtain clinical relationships among miR-146a, CD24 and β-catenin, we first checked the correlation between miR-146a and CD24expression across the NCI-60 cell lines and found it to be significantly negatively correlated (Fig.3e). Moreover, examination of $CD44^{high}$ HNSCC tumors from TCGA dataset revealed a positive correlation between miR-146a expression and β-catenin/CD24 ratio (Fig. 3f). Further, the observed down-regulation of E-cadherin upon miR-146a expression prompted us to address the miR-146a driven EMT phenomenon in OSCC. Indeed, miR-146a was found to be significantly over-expressed in the mesenchymal (MS) cell lines showing higher CD44 and lower CD24 expression[3], compared to the epithelial (EP) cell lines of the NCI-60 panel[29](Fig.3g). In addition, the miR-146a expression in TCGA tumor samples was negatively correlated with the E-cadherin to Vimentin ratio (Fig.3h). Based on these observations, we propose that miR-146a induced stemness and EMT in OSCC is mediated through lowering of CD24 followed by activation of β-catenin.

MiR-146a targets CD24 in oral CSCs

We considered CD24 as a putative target of miR-146a through which it might impart stemness in OSCC. Although, *in silico* identification of miRNA targets using the prediction software did not reveal CD24

as the probable target, we did find matching of miR-146a seed sequence in the CD24 3'UTR in miRANDA (Supplementary file 2). Despite one mismatch, the maximum free energy of miRNA-mRNA binding was favourable enough for hybridization and targeting (Figure S4a). In Fig. 2c, we had already examined that CD24 expression was significantly depleted upon miR-146a transfection in a dose dependent manner in SCC036, SCC131 and SCC084 cells. Alongside, it was up-regulated upon inhibition of miR-146a in SCC131 cells (Fig.4a). We also observed remarkable changes in CD24 transcripts in both SCC131 and SCC084 upon modulation of miR-146a (Fig.4b,c).To further confirm that CD24 is a direct target of miR-146a, we co-transfected luciferase reporter vector containing the 3'UTR fragment of CD24 gene with either miR-146a expressing vector or anti-miR-146a in SCC131 cells. As shown in Fig.4d, e and f, miR-146a over-expression reduced the luciferase activity of CD24 3'UTR, while miR-146a inhibitor elevated the same. On the contrary, transfection with mutated mir-146a did not alter the CD24 3'UTR luciferase activity significantly (Fig.4d, Figure S4b). Thus, this data experimentally validates the ability of miR-146a to directly target CD24 gene by binding to its 3'UTR. This justifies the involvement of miR-146a in negative regulation of CD24 expression in oral cancer stem cells.

Mir-146a stabilizes β-catenin by down-regulating CD24

To get a mechanistic insight into the miR-146a mediated β-catenin stabilization, CD24 was over-expressed in miR-146a over-expressing cells. Interestingly, CD24 not only abolished the stemness markers but also the expression of β-catenin and CD44 (Fig.5a and FigureS5a).This indicated that down-regulation of CD24 by miR-146a was instrumental in maintaining the high β-catenin levels and consequently the downstream stemness phenotype. This was further exemplified as CD24 over-expression alone could lead to degradation of β-catenin protein and the associated stem cell markers, while the siRNA mediated knockdown of CD24 showed an opposite effect (Fig.5b,c). Wnt target genes such as *C-myc, CD44, CCND1* were detected at conspicuous levels upon CD24 knockdown, whereas significantly depleted upon CD24 over-expression in cells expressing miR-146a (Figure S5b, c). These observations suggest an inverse correlation between CD24 and β-catenin signalling in OSCC cells. It was further confirmed by the inhibition of miR-146a-induced β-catenin nuclear mobilization upon

ectopic expression of CD24 (Figure S5d). In addition, miR-146a driven increased wnt reporter activity was found to be reduced upon CD24 over-expression (Fig.S5e). To further investigate its downstream effect on stemness phenotype, we performed an *in vitro* sphere-formation assay. We observed a considerably defective spheroid forming ability of miR-146a transfected cells in the presence of CD24 (Fig.S5f). Together, these observations suggest the possible contribution of CD24 in regulating Wnt pathway through β-catenin, thereby affecting CSC-like traits.

Involvement of pAKT in CD24 mediated degradation of β-catenin

Next, to elucidate the cause of β-catenin reduction in the presence of CD24, we treated SCC084 and SCC036 cells with MG132, and found β-catenin levels returned to that of un-transfected controls (Fig.5d). This confirms that unlike Numb, CD24 degrades β-cateninin a proteasomally dependent manner. The restored β-catenin also re-established the expression of stem cell marker Oct4 irrespective of CD24 over-expression in both SCC036 and SCC084 cells (Fig.5d). E-cadherin levels, however, remained high in the presence of CD24, irrespective of β-catenin stability (Fig.5d). Notably, CD24 did not affect Numb expression, corroborating the independent participation of CD24 in regulating β-catenin (Figure S6a). To gain mechanistic insights into the CD24 mediated β-catenin degradation, we speculated that CD24 might sequester β-catenin into the membrane bound lipid rafts analogous to that of E-cadherin[39]. To address this, we checked the CD24 and β-catenin interaction at protein level but did not found them in co-immunoprecipitation (Figure S6b). Alternatively, CD24 may also lead to β-catenin destabilization via AKT-GSK-3β pathway[40,41]. Towards this, we did find that CD24 over-expression rescued the miR-146a mediated increase in pAKT (Ser 473) activity (Fig.5e). Here it was appreciably noted that over-expression of CD24 lead to the down-regulation of total AKT protein itself and thereby phopho-AKT (Figure S6c), although it remained stable during MG132 treatment (Figure S6d). On the contrary, knockdown of CD24 in SCC036 increased pAKT and β-catenin levels (Fig.5f). Moreover, pAKT was found to be accumulated in the $CD44^{high}CD24^{low}$ fraction of SCC25 cells thereby indicating its prior involvement in stemness (Figure S6e). In addition, we observed significant depletion of β-catenin upon treatment with pAKT inhibitor (LY294002) which again confirmed its regulation by miR-146a-CD24-pAKT loop (Fig.5g).

These cell line related observations was further validated using mouse xenograft model. To check the effect of miR-146a on *in*-vivo tumor formation, SCC084 cells harboring either an empty vector (SCC084/EV) or stably expressing miR-146a (SCC084/miR-146a), were generated and the over-expression of miR-146a with subsequent downregulation of CD24 was confirmed by both qRT-PCR and western blot analysis (Fig. S7a, b and c). SCC084/EV and SCC084/miR-146a cells were then introduced in the right and left flanks of NOD/SCID mice respectively and allowed to form subcutaneous tumor (Fig S7d and e). A significant increase in tumor volume and tumor weight was observed in SCC084 xenografts stably over-expressing miR-146asuggesting enhanced stemness potential of these cells. (Fig 6a and b). Further, to explore the effect of AKT signaling on miR-146a induced tumor, mice with palpable tumors generated from SCC084/EV and SCC084/miR-146a cells were treated with quercetin,a known PI3K/AKT signalling pathway blocker [42] (Fig S7d and e). As expected, the tumor formation ability of miR-146a cells was significantly attenuated *in vivo* upon administration of quercetin at regular intervals (Fig 6a and b). While there was no effect of quercetin on miR-146a and CD24 levels, β-catenin over-expression in miR-146a tumors was compromised in presence of quercetin (Fig S7f, g). In order to investigate the effect of CD24 upon the acquired stemness of miR-146a expressing cancer cells *in vivo*, we examined xenograft tumors generated from SCC084/miR-146a cells harboring CD24 expression construct (Fig S7a, b, c, h and i). Notably, compared to the control tumors, volume and weight of CD24expressingSCC084/miR-146a tumors were not significantly (p-value = 0.7360) altered (Fig 6c and d) suggesting loss of miR-146a driven stemness. Xenograft tumor subjected to qRT-PCR analysis confirms the overexpression of miR-146a and CD24 in these cells while β-catenin is down-regulated (Fig.S7j and k). Collectively, these results indicate that CD24/AKT/β-catenin axis plays an important role in miR-146a regulated CSC-mediated tumor growth in-vivo. This was further supported by the soft agar tumorigenesis assays, which clearly showed that CD24 over-expression or AKT inhibition, both rescued the miR-146a induced colony formation in OSCC cells (Fig. S8a and b). The above results strongly prove CD24 as a negative regulator of β-catenin/Wnt signaling pathway through AKT inhibition.

β-catenin transactivates miR-146a expression contributing to positive feedback loop

The upstream regulators of miRNAs have always been involved in feedback regulatory mechanisms and are not much investigated. Analysis of miR-146a promoter has revealed the binding sites for NF-κB, TCF4/β-catenin and STAT3, suggesting possible transcriptional modulation[21,43,44].β-catenin enhances stemness features by driving the intracellular levels of c-myc and other yamanaka factors (Fig.7a). This apparently contributes to the enhanced tumorigenic properties in response to high miR-146a levels. Interestingly, we found that β-catenin also promotes the expression of miR-146a, which might augment the stemness acquiring ability of the cancer cells (Fig.7a). However, expression of miR-146a was significantly reduced in the presence of both dnTCF4 and Numb which inhibits β-catenin binding to the promoter and degrades it respectively (Fig.7b). Change in miR-146a promoter activity under similar conditions suggests that β-catenin is involved in trans-activation of miR-146a promoter (Figure S9a). We hypothesize that β-catenin mediated induction of miR-146a contributes to β-catenin mediated CD24 reduction (Fig.7a). ChIP-qPCR assay confirmed that β-catenin binds to miR-146a promoter *in vivo* (Fig.7c). Further, the recruitment of β-catenin was found to be significantly enhanced in absence of CD24 (Fig.7c). Moreover, miR-146a promoter activity was significantly increased in presence of miR-146a, while reduced upon ectopic expression of CD24 (Fig. 7d). However, the constructs with either mutated or deleted TCF4 binding sites showed no significant difference in promoter activity (Figure S9b). This may be due to the alternating levels of β-catenin which shoots up in miR-146a over-expression condition and gets depleted in presence of CD24. Transient ChIP assays with the same luciferase constructs also confirmed that β-catenin indeed binds to miR-146a promoter, which is impeded upon CD24 over-expression (Fig. 7e). These data positively confirm the feedback activation loop by β-catenin that further trans-activates miR-146a expression to shift the equilibrium towards CSC maintenance.

Discussion

Oral cancer progression has been largely attributed to both genetic and epigenetic heterogeneity. Tumorigenic cells can arise from the non-tumorigenic cancer cells owing to spontaneous conversion to a stem-like state[45]. The origin and plasticity of such cells, called cancer stem cells (CSCs), have always

been a matter of debate. Nevertheless, CSCs are known to be responsible for chemo-resistance, tumor recurrence and metastasis. Detail molecular characterization of CSCs is therefore of paramount importance for eliminating them from its roots. CD24 has been routinely used with CD44 for the prospective isolation of CSCs in colorectal, prostate and breast cancers [46]. Given the critical role of cellular miRNAs in regulating CSC characteristics, current anticancer therapies have provided an important avenue towards exploiting them for effective cellular targeting[47]. Targeting of CD44 by miRNAs in NSCLC, prostate and ovarian cancer has been previously demonstrated to attenuate stemness[17,48,49]. However, miRNA mediated regulation of CD24 remains to be determined.

Consistent with its oncogenic functions, miR-146a promotes symmetric division of colorectal CSCs, thereby promoting stemness [21]. The miRNA is also involved in development of melanoma by activating Notch1 signaling leading to drug resistance [50]. However, little is known about its role in regulating expression of CSC-related CD markers in oral cancer. In the present study, we detected significantly higher expression of miR-146a in $CD44^{high}CD24^{low}$ population of OSCC cell lines as well as in tumor specimens. We therefore speculated whether miR-146a expression maintains CSC traits or miR-146a accumulation is a consequence of induced stemness. Notably, ectopic expression of miR-146a induce CSC-phenotype i.e. $CD44^{high}CD24^{low}$ population together with increased β-catenin activity in OSCC cell lines. CD44 is a well-known transcriptional target of β-catenin along with C-myc and CCND1[21], which clearly indicates a molecular link with miR-146a induced CD44 expression. However the effect of miR-146a upon CD24 expression under these conditions was particularly intriguing. Hence, we examined whether CD24 is a direct target of miR-146a and experimentally confirmed that miR-146a binds to the 3'UTR of CD24 thereby repressing it post-transcriptionally. Loss of E-cadherin upon miR-146a over-expression and positive correlation with the mesenchymal marker vimentin was also evident. Hence, in addition to its novel role in acquiring stemness, our results re-confirmed miR-146a as a key regulator of EMT[51].

Wnt/β-catenin has shown great potential for CSC-targeting in cancer[37]. Our study shows that CSC characteristics in OSCC is attributed to the elevated β-catenin along with depleted CD24. The anticipation that CD24 leads to proteasomal degradation of β-catenin was found to be true and

apparently it also abolished the β-catenin mediated stemness. This is a novel functional interaction through which miR-146a regulates β-catenin in oral cancer cells. Our study, thus points towards the tumor-suppressor functions of CD24, supporting our previous observation of reduced CD24 expression in oral tumors compared to the normal tissue (our own data) [3]. Although growth inhibition was achieved by knocking down CD24 in colorectal and pancreatic cancer[52], no such effects were observed in oral cancer. Perhaps the variable cell-type specific distribution pattern underlies the paradoxical role of CD24 in oral cancer[53]. Activated PI3K-AKT pathway is one of the primary events in carcinogenesis[54]. Its contribution to stem cell self-renewal and proliferation (both normal and cancer) has also been extensively studied[55]. Receptor Tyrosine Kinase (RTKs) mediated growth signals (through EGF, IL-6, TGF-β etc.) impinges upon AKT through activation of the PI3K kinase[56]. Stability of phospho-AKT and other kinases play key role in maintaining cancer stem cells of chronic myeloid leukemia (CML), NSCLC, breast, prostate and colorectal cancer[55]. Further, signaling pathways like WNT are often linked with AKT activation that eventually contribute to expression of stem cells-related factors, chemo-resistance genes, and CSC markers[54,57]. Here we show that CD24, the cell surface CSC marker lie upstream of AKT protein, similar to that of TWIST and FOXO transcription factors which is also known to inhibit CD24[40,58-60]. However, the precise mechanism by which expression/stability of AKT protein is regulated by CD24 is unknown.CD24 has been shown to possibly modulate phospho-AKT levels [61], which might affect its downstream targets such as GSK-3β[41]. Activated GSK-3β mediates phosphorylation and ubiquitination of β-catenin, thereby leading to its degradation [41]. Therefore, it was incumbent on us to ask whether CD24 induce AKT and subsequently affect β-catenin stability in miR-146a induced oral CSCs. Indeed, MG132 treatment was found to re-stabilize β-catenin by relieving pAKT inhibition in cells over-expressing CD24. Moreover, direct AKT inhibition in the miR-146a transfected cells depleted β-catenin, irrespective of CD24 level suggesting AKT is downstream of CD24. Thus, we logically elucidated the molecular mechanism underlying CD24 mediated β-catenin degradation in oral cancer cells. We have specifically shown that CD24 over-expression decrease levels of phospho-AKT leading to β-catenin instability. The role of miR-146a/CD24/AKT/β-catenin axis in

maintaining the oral cancer stem cell populations is thus mechanistically evident. Studies from in-vivo tumor model system also confirms that these molecular mechanisms directly affect tumorigenesis.

Further, the recruitment of β-catenin onto miR-146a promoter was found to be negatively regulated by CD24 which might contribute to the fine tuning of stemness. These results clearly establish a cross-regulatory network between miR-146a and β-catenin, governed by a stem-related marker, CD24 in OSCC cells. Our study thus provides strong evidences which suggest that miR-146a promotes CSC characteristics of oral cancer cells by down-regulating CD24.Repression of CD24 leads to AKT stabilization followed by activation of Wnt/β-catenin signaling. Based on our observation, we propose a model wherein, AKT activity is an important determinant of miR-146a dependent β-catenin signaling (Fig.8). It should be noted, however, that β-catenin mediated CSC induction might be due to the induction of miR-146a expression or vice-versa. Taken together, the present study highlights a novel mechanism of miR-146a mediated self-renewal capacity of Oral CSCs that may have a prognostic or therapeutic value in oral cancer.

Materials and methods

Cell culture and transfection

Various human Oral Squamous Cell Carcinoma (OSCC) cell lines SCC131, SCC084 and SCC036 were obtained from Dr. Sussane Gollin, University of Pittsburgh. These cells were maintained in 5% CO_2 at 37°C in DMEM medium supplemented with 10% fetal bovine serum (FBS) and antibiotics (Life Technologies, Thermo Fisher Scientific Inc., MA, USA). The ATCC (American Type Culture Collection) oral cancer cell line, SCC25 was cultured in complete DMEM-F12 medium and 400ng/ml Hydrocortisone (Sigma Aldrich) under similar conditions. For transfection, Lipofectamine™ 2000 (Invitrogen) was used in serum free medium. Transfected cells were harvested after 48 hrs or 72 hrs for over-expression or knockdown studies respectively.

Plasmid constructs, miRNA inhibitors and siRNAs

We obtained mir-146a and mir-146a SDM expressing pU61 construct from Dr. Nitai. P. Bhattacharjee (SINP, Kolkata). The TOP-flash/FOP-flash reporters, dnTCF4, Numb, and pcDNA3.1 empty vector along with miR-146a promoter LucA, LucB and mLucA Luciferase constructs were kind gifts from Muh-Hwa Yang (Taiwan). Human CTNNB1 expression plasmid deposited by Eric Fearon was purchased from Addgene (#16828). CD24 cDNA cloned into the pCDNA3.1 vector and the full-length 3'-UTR of CD24 cloned into the HindIII site of pMIR (Ambion) were obtained from Heike Allgayer (University of Heidelberg, Germany). Anti-miR-146a (AM-34a) (ID: AM11030) were obtained from Ambion, CD24 siRNA (a pool of 3 target specific siRNAs) and Scramble siRNA from Santa Cruz. CTNNB1 shRNA constructs (Addgene # 18803) were provided by Dr. Mrinal Kanti Ghosh, IICB, Kolkata. MiR-146a over-expression cassette was sub-cloned from pU61 into the pLKO.1 TRC vector (Addgene plasmid # 10878). Packaging plasmids psPAX2 (Addgene plasmid # 12260) and pMD2.G (Didier Trono, Addgene plasmid# 12259) was used to generate the miR-146a over-expression lentiviral particles and target cells were infected following the manufacturer's protocol. Stable transduced cells were selected by puromycin (Gibco) and over-expression efficiencies were verified by qRT-PCR and western blotting. CD24 was co-transfected and clones were selected by G418.

Quantitative Real Time PCR

TRIzol (Invitrogen, Thermo Fisher Scientific Inc., MA USA) method was used for isolation of total RNA as per manufacturer's instructions. 250 ng of RNA were converted to cDNAs using stem-loop primers specific for reverse transcription of individual miRNAs[28]. MiRNA cDNAs were amplified with forward primers specific for individual miRNAs and a URP, with U6 snRNA as an endogenous reference control. For mRNA expression changes, protocol was similar to that described previously [3]. SYBR Green master mix (Roche, USA) was used to carry out qRT-PCR in the 7500 Fast Real-Time PCR instrument (Applied Biosystems, USA). Fold change values ($2^{-\Delta\Delta CT}$) were calculated from average of three independent experiments. Primer sequences of genes, miRNA forward and loop primers are listed in Supplementary File 3.

Analysis of TCGA and NCI-60 datasets

RNA and miRNA-seq data were acquired for a total of 292 HNSCC tumor specimens from TCGA (The Cancer Genome Atlas) data portal (https://tcga-data.nci.nih.gov/tcga/). We first grouped top 25% of CD44 high and low expressing tumors and then further sub-grouped 25% of these tumors based on CD24 expression (Supplementary File 1). These were designated as $CD44^{high}CD24^{low}$ and $CD44^{low}CD24^{high}$, wherein we checked the differential expression of miR-146a and calculated statistical significance using R Limma Package. Node status of these patients was also correlated with miR-146a expression using GraphPad Prism5 software. NCI-60 miRNA expression dataset (GEO accession number GSE26375) was analyzed to compare the miR-146a expression between the epithelial and mesenchymal groups as classified earlier [29] using Mann Whitney's u test.

Flow cytometry

Briefly, 48 hours post transfection of miR-146a, approximately $1x10^6$ cells were harvested in 1X PBS consisting of 1% FBS and 0.02% sodium azide. CD44-PE and CD24-FITC (BD Pharmingen) conjugated antibodies were used for double staining. Cells were then washed and subjected to flow cytometry on the BD LSRFortessa and analysis was done using BD FACSDiva 6.2 software. Debris and clumps were excluded and the size gate was decided using forward and side scatter analysis of unstained cells. Isotype controls were included for the non-specific staining.

Sphere forming assay

MiR-146a transfected cells were cultured overnight. Next day, cells were trypsinised and a single cell suspension was ensured. Low attachement 6-well plate were used for re-seeding the cells at a density of 5000 cells/ml in DMEM-F-12 serum free media containing 1% B27 supplement, 20 ng/ml of EGF and 20 ng/ml of bFGF (Invitrogen). 500 µl of media was added every 2-3 days. Photographs of the spheres were taken under inverted microscope (Leica TCS SP8; Germany) with 20X magnification at 7-14 days. All experiments were done in biological triplicates.

Immuno-fluorescence

Sorted populations of SCC131 were grown on cover-slips overnight and then fixed with chilled aceto-methanol (1:1). 0.03% Saponin (Calbiochem, Germany) was used for permeabilization followed by blocking with 3% BSA. Rabbit monoclonal antibody against β-catenin and mouse monoclonal antibody against CD24, CD44 (Cell signaling technology) were added at a dilution of 1:200 and incubated overnight. It was then probed with anti-rabbit-FITC and anti-mouse Alexa-Flour 633nm conjugated secondary antibody (molecular probes) and counter stained with DAPI (Invitrogen) for nuclear staining. Images were taken under a confocal microscope (Andor Spinning Disc Confocal Microscope, Andor Technology, Belfast, Ireland) at 60X magnification.

Western blotting

Cell lysates were prepared after 48 hrs of transfection in NP-40 lysis buffer (Invitrogen) and protease inhibitor cocktail (1X) was added for enhanced protein stability. Bradford reagent (Sigma) was used to determine concentrations and equivalent amounts of denatured protein samples were subjected to SDS-PAGE (8%-10%), separated by size and transferred on to PVDF membrane (Millipore, Billerica, USA). Antibodies used for immuno-blotting were polyclonal β-catenin, E-cadherin, CD44 and CD24, Involucrin (Santa Cruz Biotechnology, CA, USA), polyclonal Oct4 and Sox2 (Abcam), polyclonal C-myc, Akt and phospho-Akt (Cell Signaling Technology, USA). Bands were obtained using ECL substrate (Thermo Scientific, USA) from HRP-conjugated secondary antibody (Sigma). Proteasome Inhibitor MG132 (Calbiochem) and Akt inhibitor LY294002 (Cell signaling Technology, USA) were both used at a concentration of 50 µM. Transfected cells were treated for 4 hours before harvesting. Band intensities of each protein were analyzed by ImageJ to obtain densitometric values for their quantification. These were normalized to β-actin for individual experimental sets and fold change calculated. All the histograms were expressed as means ± S.D. of three different experiments and p values computed in GraphPad Prism 5 (Student's two tailed t test).

***In vivo* tumor xenograft experiments**

Animal experiments were performed following guidelines of the institutional animal ethics committee of National Centre for Cell Science, Pune. All the animals were issued under the project

IAEC/2012/B183. To investigate the effect of miR-146a overexpression on Oral squamous cell carcinoma (OSCC) growth *in vivo*, 3×10^6 empty vector- and microRNA overexpression construct-containing SCC084 cells were injected subcutaneously into the dorsal flanks of eight NOD/SCID male mice (18 weeks old) on left and right side respectively. When palpable tumors could be seen the mice were segregated into groups of four each. Mice in one of the groups were injected with 25 mg/kg of body weight of Quercetin (Sigma) on every alternate day for a period of 15 days. The experiment was terminated when the average miR-146a over-expressing SCC084 tumor volumes in the group which received no quercetin reached about 1200 mm^3. At the termination of the experiment, the animals were sacrificed by CO_2 asphyxiation and the tumors were collected for further analysis. Tumor diameters were measured each time the Quercetin was injected and at the termination of the experiment using digital Vernier Caliper. Excised tumor tissues were weighed and then stored in RNAlater solution (ThermoFisher Scientific) in -20°C freezer. Tumor volumes were determined using the following formula: $\pi/6[(d1\times d2)^{3/2}]$; where d1 and d2 are two different diameters of a tumor. In another experiment, to investigate effect of simultaneous overexpression of miR-146a and CD24 on OSCC growth *in vivo*, 3×10^6 empty vector- and miR-146a and CD24 overexpression constructs-containing OSCC-084 cells were injected subcutaneously into the dorsal flanks of four NOD/SCID male mice (15 weeks old) on left and right side respectively. Tumors volumes were measured when palpable growth could be observed. The experiment was terminated when tumor volumes reached 1300 mm^3. The animals were euthanized by CO_2 asphyxiation and the tumors were collected. Tumor tissues were processed as described previously for the other experiment.

Reporter assays

Cells seeded in 24 well plates were co-transfected with miR-146a OE plasmid and either CD24 3'UTR or miR-146a promoter luciferase construct using Lipofectamine™ 2000 (Invitrogen). The TOP-Flash and FOP-Flash reporters were also used under similar conditions. Promega dual luciferase assay system was performed according to the manufacturer's protocol. After 48 hr of transfection, medium was washed off with 1x PBS and cells were lysed with Passive Lysis Buffer (Promega) and luminescence was measured in Promega Glomax 20/20 luminometer. The luminescence values were transfection

normalized with the internal control pRL-TK (50 ng, Renilla Luciferase; Promega). Experiments were performed with three biological replicates.

Chromatin immunoprecipitation

Cells seeded in 10cm dishes were transfected. After 48hrs, 1X formaldehyde solution was added for DNA-protein crosslinking. Cells were lysed in SDS lysis buffer followed by sonication in Bioruptor (Diagenode) to obtain 200-1000 bp chromatin fragments. ChIP dilution buffer was used to dilute the sheared chromatin followed by preclearing with Protein G Agarose beads (Sigma) for 30min. After preclearing, 20% of the lysate was kept aside as the input and the remaining was divided equally for IP and IgG. Immunoprecipitation was carried out using 5µg of β-catenin (Santa Cruz) and normal IgG control (Sigma) and incubated overnight. The following day, Protein G Agarose beads were added to collect the Antibody/Antigen/Chromatin complex. The complex was washed briefly with cold low salt immune complex wash followed by high salt immune complex buffer, lithium chloride immune complex buffer and Tris-EDTA buffer. It was then reverse-crosslinked and the DNA purified using Phenol/Chloroform extraction method. PCR amplification of the immunoprecipitated DNA was carried out using primers listed in Supplementary File 1. Composition of the ChIP buffers are provided in Supplementary Information.

Statistical analyses

Three different experiments were subjected to an independent two-tailed Student's *t* test to measure the significance value of results under varying biological parameters. R package was used to generate the correlation graphs and calculate p values. * indicates $P \leq 0.05$ and ** indicates $P \leq 0.01$.

Supplementary information

Supplementary Figure and Figure Legends (S1, S2, S3, S4, S5, S6, S7, S8, S9)

Supplementary methods

Supplementary File 1: Analysis of TCGA data for Head and Neck Squamous Cell Carcinoma patients (Excel File)

Supplementary File 2: Snapshots of miRANDA analysis for miR-146a-5p seed sequence and CD24 3'UTR matching showing their free energy of binding (pdf)

Supplementary File 3: List of Primers for the qRT-PCR (Excel File)

Acknowledgements

We thank Prof. Nitai. P. Bhattacharjee (SINP), Dr. Muh-Hwa Yang (National Yang-Ming University, Taiwan) and Dr. Heike Allgayer (University of Heidelberg, Germany) for providing us the necessary plasmids. We thank Dr. Raghunath Chatterjee (Indian Statistical Institute, Kolkata, India) for performing the RNA-hybrid analysis in miRANDA software. We thank Tanmoy Dalui and Diptadeep Sarkar (CSIR-Indian Institute of Chemical Biology, Kolkata, India) for helping us with FlowCytometry and Confocal Microscopy respectively. We thank Dr. Arindam Datta (CSIR-Indian Institute of Chemical Biology, Kolkata, India) for assisting TCGA and NCI-60 dataset analysis. The work was supported by CSIR—Mayo Clinic Collaboration for Innovation and Translational Research Grant CMPP-08 and J.C. Bose National Fellowship grant JCB/2017/000005 awarded to S. Roychoudhury. S.G, D.G and P.D. are supported by fellowship from the Council of Scientific and Industrial Research (New Delhi, India). Mouse experiments and SD, RB and MG are supported by CSIR- fellowship in NCCS, Pune.

Author contributions

SG and SR conceived and designed the study. Some experiments were designed by DG and SD. Experiments, data collection and statistical analyses were performed by SG, DG, SD and PD. Some experiments were performed by RB and MG. The manuscript was written and edited by SG, DG, SD, GC and SR. All authors read and approved the final manuscript.

Conflict of interest

The authors declare that they have no conflict of interest.

References

1 Suh, Y., Amelio, I., Guerrero Urbano, T. & Tavassoli, M. Clinical update on cancer: molecular oncology of head and neck cancer. *Cell death & disease* **5**, e1018, doi:10.1038/cddis.2013.548 (2014).

2 Smith, B. A. *et al.* A basal stem cell signature identifies aggressive prostate cancer phenotypes. *Proceedings of the National Academy of Sciences of the United States of America* **112**, E6544-6552, doi:10.1073/pnas.1518007112 (2015).

3 Ghuwalewala, S. *et al.* CD44(high)CD24(low) molecular signature determines the Cancer Stem Cell and EMT phenotype in Oral Squamous Cell Carcinoma. *Stem cell research* **16**, 405-417, doi:10.1016/j.scr.2016.02.028 (2016).

4 Prince, M. E. *et al.* Identification of a subpopulation of cells with cancer stem cell properties in head and neck squamous cell carcinoma. *Proceedings of the National Academy of Sciences of the United States of America* **104**, 973-978, doi:10.1073/pnas.0610117104 (2007).

5 Munoz, P., Iliou, M. S. & Esteller, M. Epigenetic alterations involved in cancer stem cell reprogramming. *Molecular oncology* **6**, 620-636, doi:10.1016/j.molonc.2012.10.006 (2012).

6 Lund, A. H. & van Lohuizen, M. Epigenetics and cancer. *Genes & development* **18**, 2315-2335, doi:10.1101/gad.1232504 (2004).

7 Sharma, S., Kelly, T. K. & Jones, P. A. Epigenetics in cancer. *Carcinogenesis* **31**, 27-36 (2010).

8 Calin, G. A. & Croce, C. M. MicroRNA signatures in human cancers. *Nature reviews. Cancer* **6**, 857-866, doi:10.1038/nrc1997 (2006).

9 Courthod, G., Franco, P., Palermo, L., Pisconti, S. & Numico, G. The role of microRNA in head and neck cancer: current knowledge and perspectives. *Molecules (Basel, Switzerland)* **19**, 5704-5716, doi:10.3390/molecules19055704 (2014).

10 Min, A. *et al.* MicroRNAs as Important Players and Biomarkers in Oral Carcinogenesis. *BioMed research international* **2015**, 186904, doi:10.1155/2015/186904 (2015).

11 Liu, C. & Tang, D. G. MicroRNA regulation of cancer stem cells. *Cancer research* **71**, 5950-5954, doi:10.1158/0008-5472.can-11-1035 (2011).

12 Tiwari, A., Shivananda, S., Gopinath, K. S. & Kumar, A. MicroRNA-125a reduces proliferation and invasion of oral squamous cell carcinoma cells by targeting estrogen-related receptor alpha: implications for cancer therapeutics. *The Journal of biological chemistry* **289**, 32276-32290, doi:10.1074/jbc.M114.584136 (2014).

13 Chen, D. *et al.* miR-100 induces epithelial-mesenchymal transition but suppresses tumorigenesis, migration and invasion. *PLoS genetics* **10**, e1004177, doi:10.1371/journal.pgen.1004177 (2014).

14 Yu, Z., Li, Y., Fan, H., Liu, Z. & Pestell, R. G. miRNAs regulate stem cell self-renewal and differentiation. *Frontiers in genetics* **3**, 191, doi:10.3389/fgene.2012.00191 (2012).

15 Sun, X. *et al.* MicroRNAs and cancer stem cells: the sword and the shield. *Oncogene* **33**, 4967-4977, doi:10.1038/onc.2013.492 (2014).

16 Chaffer, C. L. *et al.* Poised chromatin at the ZEB1 promoter enables breast cancer cell plasticity and enhances tumorigenicity. *Cell* **154**, 61-74, doi:10.1016/j.cell.2013.06.005 (2013).

17 Shi, Y., Liu, C., Liu, X., Tang, D. G. & Wang, J. The microRNA miR-34a inhibits non-small cell lung cancer (NSCLC) growth and the CD44hi stem-like NSCLC cells. *PloS one* **9**, e90022, doi:10.1371/journal.pone.0090022 (2014).

18 Xu, N., Papagiannakopoulos, T., Pan, G., Thomson, J. A. & Kosik, K. S. MicroRNA-145 regulates OCT4, SOX2, and KLF4 and represses pluripotency in human embryonic stem cells. *Cell* **137**, 647-658, doi:10.1016/j.cell.2009.02.038 (2009).

19 Yang, X., Ni, W. & Lei, K. miR-200b suppresses cell growth, migration and invasion by targeting Notch1 in nasopharyngeal carcinoma. *Cellular physiology and biochemistry : international*

journal of experimental cellular physiology, biochemistry, and pharmacology **32**, 1288-1298, doi:10.1159/000354527 (2013).

20 Hung, P. S. *et al.* miR-146a enhances the oncogenicity of oral carcinoma by concomitant targeting of the IRAK1, TRAF6 and NUMB genes. *PloS one* **8**, e79926, doi:10.1371/journal.pone.0079926 (2013).

21 Hwang, W. L. *et al.* MicroRNA-146a directs the symmetric division of Snail-dominant colorectal cancer stem cells. *Nature cell biology* **16**, 268-280, doi:10.1038/ncb2910 (2014).

22 Gottardi, C. J., Wong, E. & Gumbiner, B. M. E-cadherin suppresses cellular transformation by inhibiting beta-catenin signaling in an adhesion-independent manner. *The Journal of cell biology* **153**, 1049-1060 (2001).

23 Liu, Y., Huang, T., Zhao, X. & Cheng, L. MicroRNAs modulate the Wnt signaling pathway through targeting its inhibitors. *Biochemical and biophysical research communications* **408**, 259-264, doi:10.1016/j.bbrc.2011.04.009 (2011).

24 Perry, J. M. *et al.* Cooperation between both Wnt/{beta}-catenin and PTEN/PI3K/Akt signaling promotes primitive hematopoietic stem cell self-renewal and expansion. *Genes & development* **25**, 1928-1942, doi:10.1101/gad.17421911 (2011).

25 Zeng, X. C. *et al.* Downregulation of miR-610 promotes proliferation and tumorigenicity and activates Wnt/beta-catenin signaling in human hepatocellular carcinoma. *Molecular cancer* **13**, 261, doi:10.1186/1476-4598-13-261 (2014).

26 Vegfors, J., Petersson, S., Kovacs, A., Polyak, K. & Enerback, C. The expression of Psoriasin (S100A7) and CD24 is linked and related to the differentiation of mammary epithelial cells. *PloS one* **7**, e53119, doi:10.1371/journal.pone.0053119 (2012).

27 Muppala, S. *et al.* CD24 induces expression of the oncomir miR-21 via Src, and CD24 and Src are both post-transcriptionally downregulated by the tumor suppressor miR-34a. *PloS one* **8**, e59563, doi:10.1371/journal.pone.0059563 (2013).

28 Chen, C. *et al.* Real-time quantification of microRNAs by stem-loop RT-PCR. *Nucleic acids research* **33**, e179, doi:10.1093/nar/gni178 (2005).

29 Park, S. M., Gaur, A. B., Lengyel, E. & Peter, M. E. The miR-200 family determines the epithelial phenotype of cancer cells by targeting the E-cadherin repressors ZEB1 and ZEB2. *Genes & development* **22**, 894-907, doi:10.1101/gad.1640608 (2008).

30 Henson, B. J., Bhattacharjee, S., O'Dee, D. M., Feingold, E. & Gollin, S. M. Decreased expression of miR-125b and miR-100 in oral cancer cells contributes to malignancy. *Genes, chromosomes & cancer* **48**, 569-582, doi:10.1002/gcc.20666 (2009).

31 Li, J. *et al.* MiR-21 indicates poor prognosis in tongue squamous cell carcinomas as an apoptosis inhibitor. *Clinical cancer research : an official journal of the American Association for Cancer Research* **15**, 3998-4008, doi:10.1158/1078-0432.ccr-08-3053 (2009).

32 Sethi, N., Wright, A., Wood, H. & Rabbitts, P. MicroRNAs and head and neck cancer: reviewing the first decade of research. *European journal of cancer (Oxford, England : 1990)* **50**, 2619-2635, doi:10.1016/j.ejca.2014.07.012 (2014).

33 Paik, J. H. *et al.* MicroRNA-146a downregulates NFkappaB activity via targeting TRAF6 and functions as a tumor suppressor having strong prognostic implications in NK/T cell lymphoma. *Clinical cancer research : an official journal of the American Association for Cancer Research* **17**, 4761-4771, doi:10.1158/1078-0432.ccr-11-0494 (2011).

34 Shi, Z., Johnson, J. J., Jiang, R., Liu, Y. & Stack, M. S. Decrease of miR-146a is associated with the aggressiveness of human oral squamous cell carcinoma. *Archives of oral biology* **60**, 1416-1427, doi:10.1016/j.archoralbio.2015.06.007 (2015).

35 Zhang, Z., Zhang, Y., Sun, X. X., Ma, X. & Chen, Z. N. microRNA-146a inhibits cancer metastasis by downregulating VEGF through dual pathways in hepatocellular carcinoma. *Molecular cancer* **14**, 5, doi:10.1186/1476-4598-14-5 (2015).

36 Comprehensive genomic characterization of head and neck squamous cell carcinomas. *Nature* **517**, 576-582, doi:10.1038/nature14129 (2015).

37 Takebe, N. *et al.* Targeting Notch, Hedgehog, and Wnt pathways in cancer stem cells: clinical update. *Nature reviews. Clinical oncology* **12**, 445-464, doi:10.1038/nrclinonc.2015.61 (2015).

38 McGill, M. A. & McGlade, C. J. Mammalian numb proteins promote Notch1 receptor ubiquitination and degradation of the Notch1 intracellular domain. *The Journal of biological chemistry* **278**, 23196-23203, doi:10.1074/jbc.M302827200 (2003).

39 Orsulic, S., Huber, O., Aberle, H., Arnold, S. & Kemler, R. E-cadherin binding prevents beta-catenin nuclear localization and beta-catenin/LEF-1-mediated transactivation. *Journal of cell science* **112 (Pt 8)**, 1237-1245 (1999).

40 Li, J. & Zhou, B. P. Activation of beta-catenin and Akt pathways by Twist are critical for the maintenance of EMT associated cancer stem cell-like characters. *BMC Cancer* **11**, 49, doi:10.1186/1471-2407-11-49 (2011).

41 Zhao, S. *et al.* Activation of Akt/GSK-3beta/beta-catenin signaling pathway is involved in survival of neurons after traumatic brain injury in rats. *Neurological research* **34**, 400-407, doi:10.1179/1743132812y.0000000025 (2012).

42 Lim W, Y. C., Park S, Bazer FW, Song G. Inhibitory Effects of Quercetin on Progression of Human Choriocarcinoma Cells Are Mediated Through PI3K/AKT and MAPK Signal Transduction Cascades. *J Cell Physiol* **Jun;232(6)**, 1428-1440. , doi:doi: 10.1002/jcp.25637. (2017).

43 Sun, X. *et al.* miR-146a is directly regulated by STAT3 in human hepatocellular carcinoma cells and involved in anti-tumor immune suppression. *Cell Cycle* **14**, 243-252 (2014).

44 Taganov, K. D., Boldin, M. P., Chang, K. J. & Baltimore, D. NF-kappaB-dependent induction of microRNA miR-146, an inhibitor targeted to signaling proteins of innate immune responses. *Proceedings of the National Academy of Sciences of the United States of America* **103**, 12481-12486, doi:10.1073/pnas.0605298103 (2006).

45 Chaffer, C. L. *et al.* Normal and neoplastic nonstem cells can spontaneously convert to a stem-like state. *Proceedings of the National Academy of Sciences of the United States of America* **108**, 7950-7955, doi:10.1073/pnas.1102454108 (2011).

46 Jaggupilli, A. & Elkord, E. Significance of CD44 and CD24 as cancer stem cell markers: an enduring ambiguity. *Clinical & developmental immunology* **2012**, 708036, doi:10.1155/2012/708036 (2012).

47 Ling, H., Fabbri, M. & Calin, G. A. MicroRNAs and other non-coding RNAs as targets for anticancer drug development. *Nature reviews. Drug discovery* **12**, 847-865, doi:10.1038/nrd4140 (2013).

48 Cheng, W., Liu, T., Wan, X., Gao, Y. & Wang, H. MicroRNA-199a targets CD44 to suppress the tumorigenicity and multidrug resistance of ovarian cancer-initiating cells. *The FEBS journal* **279**, 2047-2059, doi:10.1111/j.1742-4658.2012.08589.x (2012).

49 Liu, C. *et al.* The microRNA miR-34a inhibits prostate cancer stem cells and metastasis by directly repressing CD44. *Nature medicine* **17**, 211-215, doi:10.1038/nm.2284 (2011).

50 Forloni, M. *et al.* miR-146a promotes the initiation and progression of melanoma by activating Notch signaling. *eLife* **3**, e01460, doi:10.7554/eLife.01460 (2014).

51 Wang, X. *et al.* Kruppel-like factor 8 promotes tumorigenic mammary stem cell induction by targeting miR-146a. *American journal of cancer research* **3**, 356-373 (2013).

52 Sagiv, E. *et al.* Targeting CD24 for treatment of colorectal and pancreatic cancer by monoclonal antibodies or small interfering RNA. *Cancer research* **68**, 2803-2812, doi:10.1158/0008-5472.can-07-6463 (2008).

53 Cremers, N. *et al.* CD24 Is Not Required for Tumor Initiation and Growth in Murine Breast and Prostate Cancer Models. *PloS one* **11**, e0151468, doi:10.1371/journal.pone.0151468 (2016).

54 Zhang, H. F. *et al.* The PI3K/AKT/c-MYC axis promotes the acquisition of cancer stem-like features in esophageal squamous cell carcinoma. *Stem cells (Dayton, Ohio)*, doi:10.1002/stem.2395 (2016).

55 Xia, P. & Xu, X. Y. PI3K/Akt/mTOR signaling pathway in cancer stem cells: from basic research to clinical application. *American journal of cancer research* **5**, 1602-1609 (2015).

56 Dubrovska, A. *et al.* The role of PTEN/Akt/PI3K signaling in the maintenance and viability of prostate cancer stem-like cell populations. *Proceedings of the National Academy of Sciences of the United States of America* **106**, 268-273 (2009).

57 Huang, T. S. *et al.* A Regulatory Network Involving beta-Catenin, e-Cadherin, PI3k/Akt, and Slug Balances Self-Renewal and Differentiation of Human Pluripotent Stem Cells In Response to Wnt Signaling. *Stem Cells* **33**, 1419-1433 (2015).

58 Ma, Y., Wang, X., Peng, Y. & Ding, X. Forkhead box O1 promotes INS-1 cell apoptosis by reducing the expression of CD24. *Molecular Medicine Reports* **13**, 2991-2998, doi:10.3892/mmr.2016.4896 (2016).

59 Vesuna, F., Lisok, A., Kimble, B. & Raman, V. Twist modulates breast cancer stem cells by transcriptional regulation of CD24 expression. *Neoplasia (New York, N.Y.)* **11**, 1318-1328 (2009).

60 Ni, Y. G. *et al.* FoxO transcription factors activate Akt and attenuate insulin signaling in heart by inhibiting protein phosphatases. *Proceedings of the National Academy of Sciences of the United States of America* **104**, 20517-20522, doi:10.1073/pnas.0610290104 (2007).

61 Hosonaga, M., Arima, Y., Sugihara, E., Kohno, N. & Saya, H. Expression of CD24 is associated with HER2 expression and supports HER2-Akt signaling in HER2-positive breast cancer cells. *Cancer science* **105**, 779-787, doi:10.1111/cas.12427 (2014).

FIGURE LEGENDS

Fig. 1. Over-expression of miR-146a in $CD44^{high}CD24^{low}$ cells of Oral Squamous Cell Carcinoma. (**a**) Total RNA extracted from the stem ($CD44^{high}CD24^{low}$) and the non-stem ($CD44^{low}CD24^{high}$) sub-populations of SCC25 cells were reverse-transcribed using stem-loop primers specific for subsequent Real time PCR analysis of various miRNAs using respective forward primers and Universal reverse primer (Additional File 1). (**b**) Expression of miR-146a was re-analyzed in UPCI: SCC131 and UPCI: SCC084 by qRT-PCR. (**c**) Quantification of miR-146a transcripts in the spheres enriched from $CD44^{high}CD24^{low}$ cells of SCC131 compared to that grown under differentiating adherent conditions. Data is representative of 3 independent experiments and the bar graph is shown with mean ± SD (right). U6snRNA was used to normalize relative expression values. Students t test used to calculate p-value (* $P<0.05$, ** $P<0.01$, *** $P<0.001$). (**d**) Box-Scatter plot showing the differential expression of miR-146a in the $CD44^{high}CD24^{low}$ and $CD44^{low}CD24^{high}$ subgroup of HNSCC tumors obtained from TCGA. (p-value was calculated in R package to show statistical significance).

672 **Fig. 2.** Cancer stem cell characteristics induced by miR-146a in OSCC cell lines. (**a**) MiR-146a
673 transfected SCC131 cells were analyzed by flow cytometry and mean fluorescence values of CD44
674 (PE) and CD24 (FITC) are shown. (**b**) Equal number of vector and miR-146a transfected UPCI:
675 SCC131 and UPCI: SCC036 cells were seeded in ultralow-attachment 6-well plate at clonal density.
676 Sphere forming structures was captured at five random fields at 20X magnification using phase contrast
677 microscope (Leica CTR4000) with scale bar equal to 50 µm. (**c**)Representative images of western blots
678 showing dose dependent increment of Sox2, C-myc, Oct-4, Involucrin and CD44, CD24 in the UPCI:
679 SCC036, UPCI: SCC131 and UPCI: SCC084 upon ectopic expression of miR-146a. β-actin bands was
680 used to normalize the data. Band intensities of each protein has been quantified from three biological
681 replicates and the average ± sd is plotted in GraphPad prism 5 showing statistical significance in the
682 respective graphs (below)(* P<0.05, **P<0.01, *** P<0.001)(**d**) Similar western blots upon
683 transfection of miR-146a with mutated seed sequences in UPCI:SCC131 and its graphical
684 representation (below).

685

686 **Fig. 3.** MiR-146a induced β-catenin/Wnt Signaling in $CD44^{high}CD24^{low}$ population. (**a**) Isolation of
687 $CD24^{low}$ and $CD24^{high}$ cells from SCC084, as shown by qRT-PCR of CD24. Western blot images of β-
688 catenin, Oct-4, E-cadherin and Involucrin in the respective populations along with its quantitative plot
689 indicating the statistical data. (**b**) Representative confocal immunofluorescence images (60X
690 magnification) of $CD44^{high}CD24^{high}$ and $CD44^{high}CD24^{low}$ subpopulation of SCC131 showing β-catenin
691 (green) and CD44 (red) counterstained with DAPI (blue) (scale bar equal to 10 µm) (**c**) Each of the
692 SCC cell lines were subjected to western blot analysis of β-catenin and E-cadherin upon increasing
693 doses of miR-146a. (**d**) β-catenin and Oct-4 immunoblotting upon increasing doses of anti-miR-146a.
694 Data normalized with β-actin. All the data has been graphically represented beneath the respective
695 figures (* P<0.05, **P<0.01, *** P<0.001) (**e**) Association of miR-146a expression with CD24 in the
696 NCI-60 cell lines (n=59) and (**f**) with β-catenin/CD24 ratio in the $CD44^{high}$ tumors of the TCGA HNSCC
697 patients (n=146). Statistical significance was determined by Pearson correlation test. Pearson
698 correlation coefficient is shown in each plot. (**g**) Box plots showing miR-146a expression in NCI-60

699 cell lines classified as epithelial (EP) and mesenchymal (MS) subgroups. p value has been calculated
700 using mann-whitney's u-test. (**h**) Correlation (Pearson) of miR-146a with CDH1/VIM expression ratio
701 based on the RNA-Seq data from 292 TCGA HNSCC specimens

702

703 **Fig. 4.** MiR-146a targets CD24 post-transcriptionally. **(a**) Immunoblotting of CD24 in SCC131 cells
704 subjected to miR-146a knockdown showing significant up-regulation upon normalization with β-actin.
705 (**b**) qRT-PCR to detect CD24 transcripts in the anti-miR-146a treated or (**c**) miR-146a over-expressed
706 SCC131 and SCC084 cells.18srRNA served as an endogenous control and p-values calculated by
707 Student's t-test. Schematic representation of the CD24 3'UTR luciferase constructs. (**d**) Luciferase
708 activity of the CD24 3'UTR reporter gene in SCC084 cells with increasing expression of miR-146a or
709 miR-SDM (mutant miR-146a). (**e**) CD24 3'UTR reporter activity upon miR-146a over-expression and
710 (**f**) miR-146a knockdown in SCC131 cells. Data in (**d**)-(**f**) are mean ±SD, normalized with pRL-TK
711 vector and statistical significance was measured by paired Student's t test (two-tailed).

712

713 **Fig. 5.** MiR-146a promotes stemness by down-regulating CD24 and leads to AKT mediated
714 stabilization of β-catenin. (**a**) Immunoblot analysis of SCC131 transfected with either a vector control,
715 miR-146a with or without CD24 showing rescued expression of β-catenin and E-cadherin as well as
716 Involucrin Oct-4, Sox2, C-myc. (**b**) Immunoblotting of the same proteins with increasing dose of CD24
717 expression and (**c**) upon knockdown of CD24 in SCC131 cells. β-actin is loaded as an endogenous
718 control. Histograms show fold changes in the densitometric values of band intensity and shown as
719 means ± S.D. of 3 individual experiments. (**d**) Western blot analysis revealed degradation of β-catenin
720 upon CD24 over-expression revived with MG132 treatment in SCC084, SCC036. (**e**) Phospho-AKT
721 levels upon miR-146a alone or in combination with CD24. Total AKT is also shown. (**f**) Phospho-AKT
722 and Total AKT levels upon siRNA mediated down-regulation of CD24 in SCC036 cells. (**g**) Effect of
723 pAKT inhibitor upon β-catenin levels in SCC084 cells. Histograms showing fold change in the

724 densitometric values of band intensity is represented as avg ± S.D. of n different experiments (n=3) (*
725 P<0.05, **P<0.01).

726

727 **Fig. 6.** MiR-146a promotes *in vivo* tumor growth which is rescued upon CD24/AKT modulation (a)
728 Bar graphs showing relative weight (mg) of the tumors xenograft tumors generated from control or
729 miR-146a expressing SCC084 treated without or with Quercetin. Data represent mean ± SEM (n=4).
730 P-values were computed using two-tailed Student's t-test. (b) Line graph showing relative growth rate
731 of tumors in response to Quercetin in SCC084 cells harboring either control vector or stably expressing
732 miR-146a. Once tumors reached a palpable size, one set of mice were injected with Quercetin (10
733 mg/kg) intraperitoneally and after 10 successive treatment, change in tumor volume was measured at
734 regular interval up to 20 days. Data represent mean ±SEM (n = 4) and *p*-values shown using Student's
735 t test. (c) Bar graphs showing relative weight (mg) of the tumors described in xenograft tumors
736 generated from SCC084 harboring either control vector or stably expressing miR146a and CD24. Data
737 represent mean ±SEM (n=4). P-values were assessed using 2-tailed Student's t-test (d) Line graph
738 showing relative growth rate of tumors described in (d). Data represent mean ±SEM (n = 4). For all the
739 experiments, *p*-values were calculated in graph-pad prism5 using two-tailed Student's t-test algorithm.

740

741 **Fig.7.** β-catenin transactivates miR-146a mediating a positive feedback loop. (**a**) Increase in stemness
742 markers upon β-catenin over-expression as revealed by western blot and the densitometric analysis of
743 its band intensities (right below). Data was normalized with corresponding β-actin. Concomitant miR-
744 146a expression in β-catenin transfected SCC131 as quantified by qPCR. (**b**) Increase in miR-146a
745 transcripts upon β-catenin over-expression is dose dependently inhibited in the presence of either
746 dnTCF4 or Numb. (**c**) Chromatin Immunoprecipitation assays in SCC084 cells transfected with either
747 scramble siRNA or CD24 siRNA showing recruitment of β-catenin upon endogenous miR-146a
748 promoter. Schematic of miR-146a promoter locus and reporter constructs namely LucA: wild-type;
749 mLucA: TCF-4 binding site (TBS) mutation; LucB: TBS deletion[21]. (**d**) Relative luciferase activity

of LucA in SCC084 cells under various transfections as indicated. Data represent average of n=3 individual experiments (along with technical replicates). (**e**) Transient ChIP assay with same constructs as shown. The percentage enrichment of amplified product was normalized to input and graphically presented. Data represent mean ± sd and n=3 different experiments (along with technical replicates*$P<$ 0.05, **$P<$ 0.01). We used Student's *t*-test calculate *p*-value.

Fig.8. Model –schematic representation of transient inter-conversions between stem and non-stem oral cancer cells. Cancer stem cell induction may be triggered with over-expression of miR-146a that targets CD24 and leads to β-catenin protein stabilization via AKT activation. Wnt signalling intermediates promote stem-like de-differentiated state in the tumor cells. Accumulation of β-catenin might further drive miR-146a expression and amplify the stemness characteristics. Stochastic intra-cellular signals may induce differentiation, probably by aberrant activation of CD24. This leads to decline in pAKT levels and hence proteasomal degradation of β-catenin with subsequent loss of miR-146a.

Figure 1

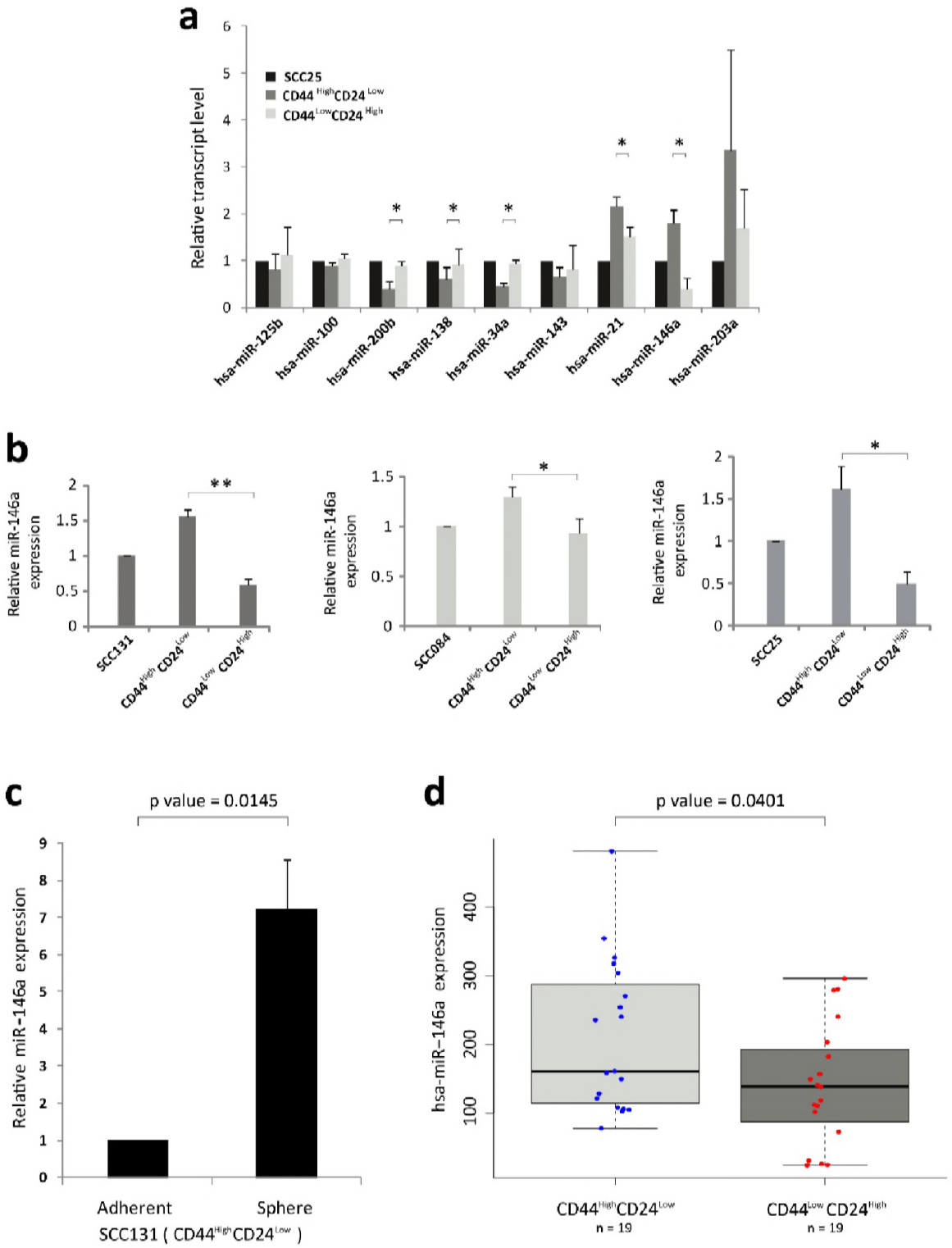

769

770

771 **Figure 2**

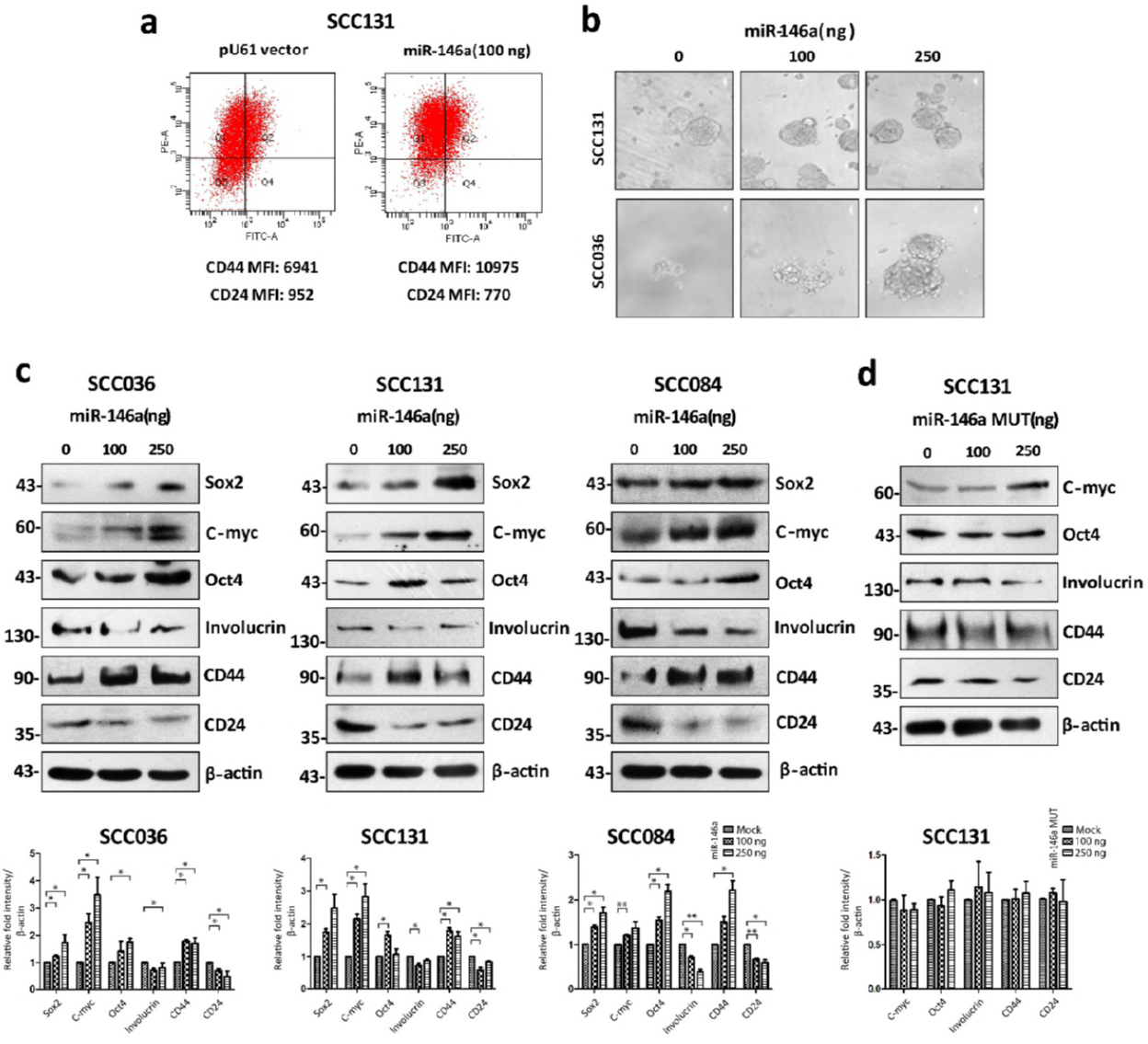

Figure 3

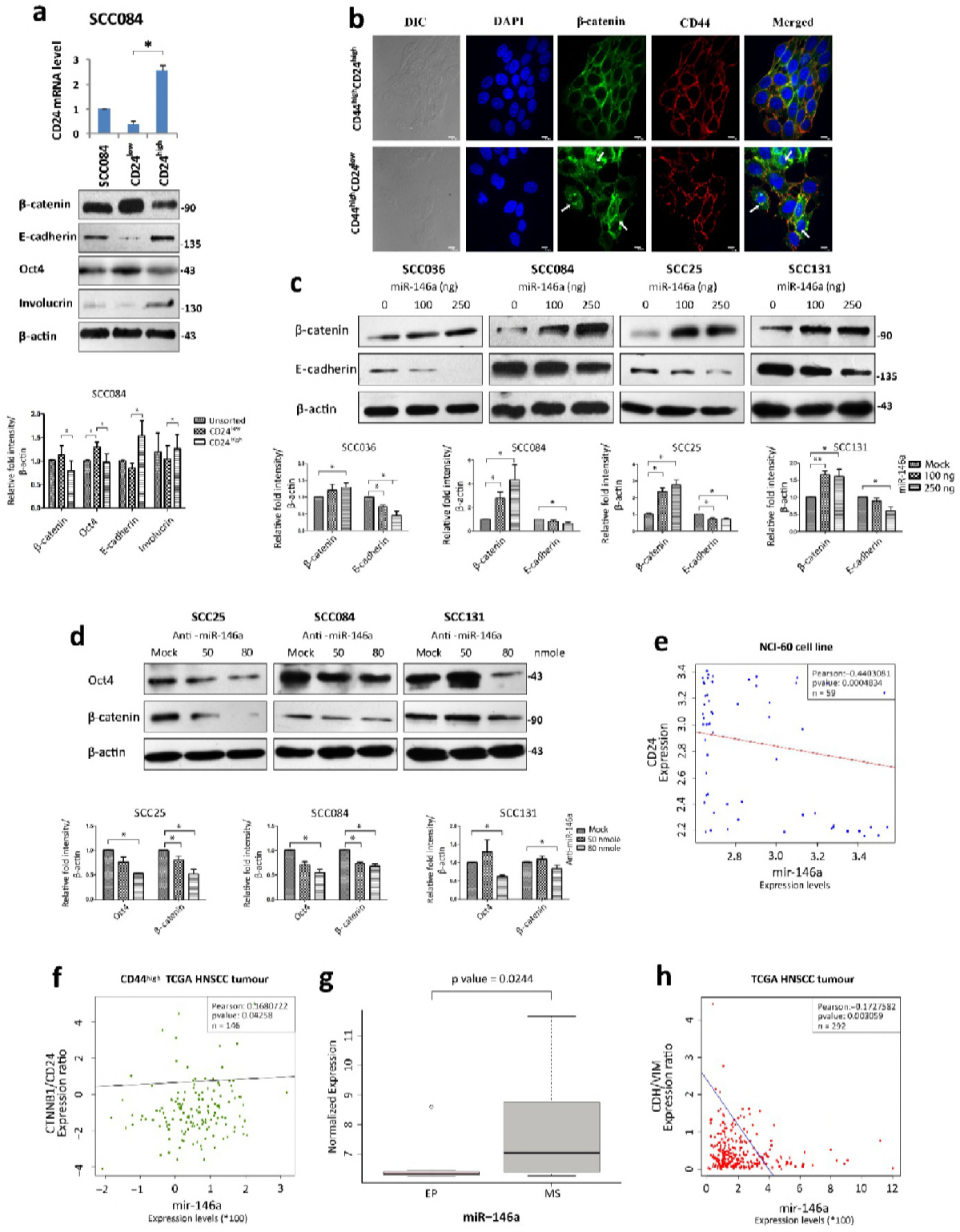

Figure 4

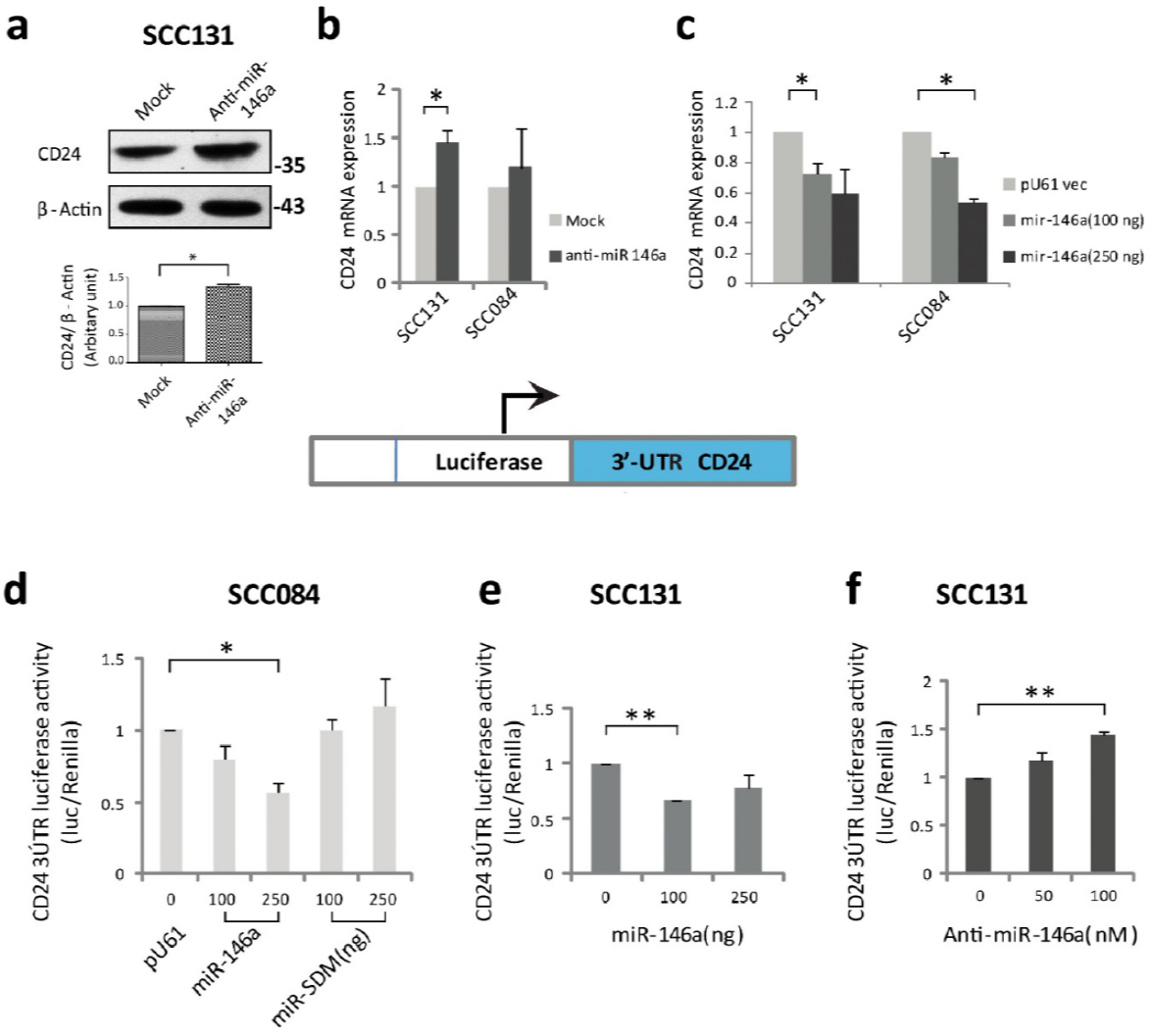

Figure 5

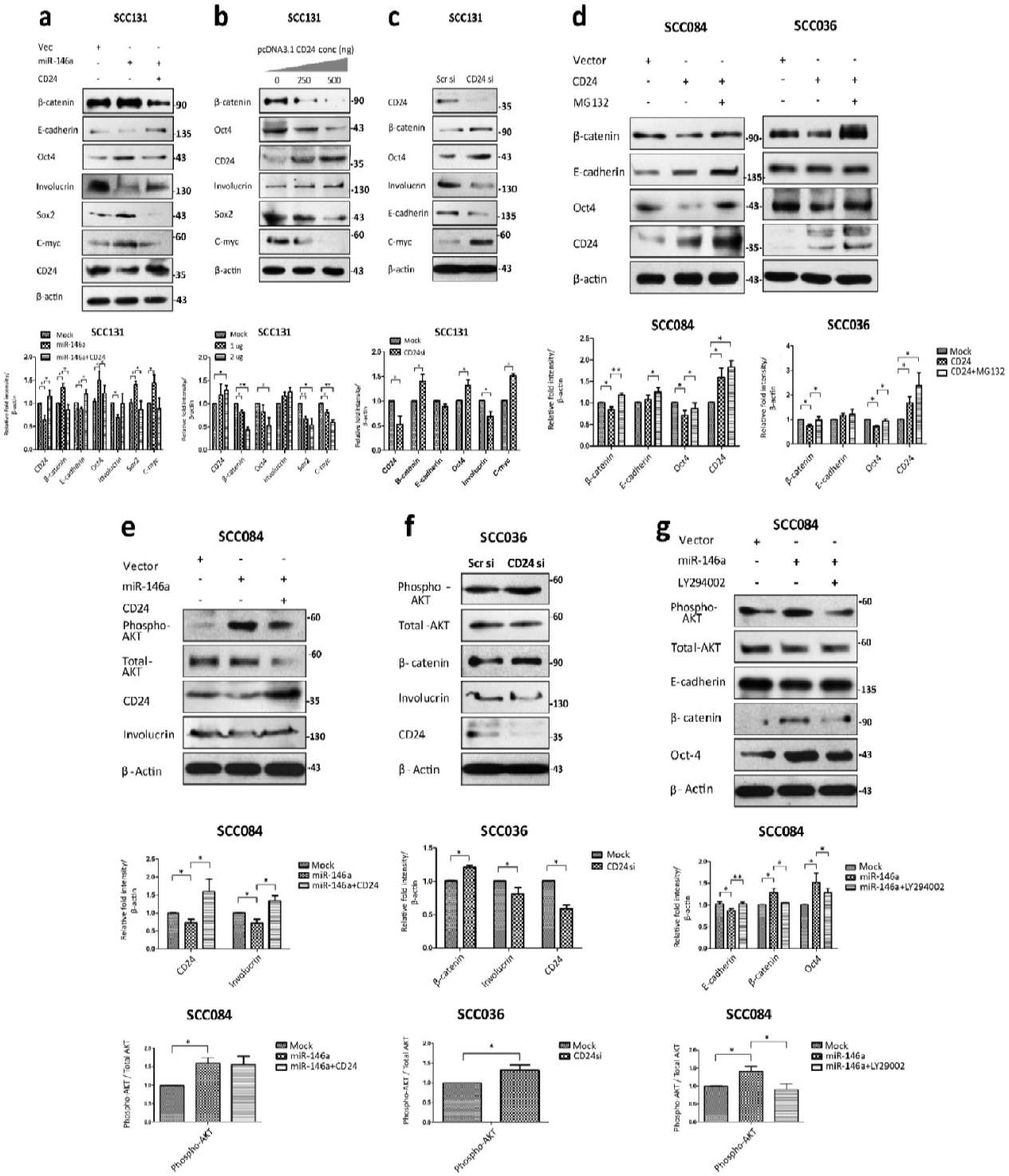

790

791

792

793 **Figure 6**

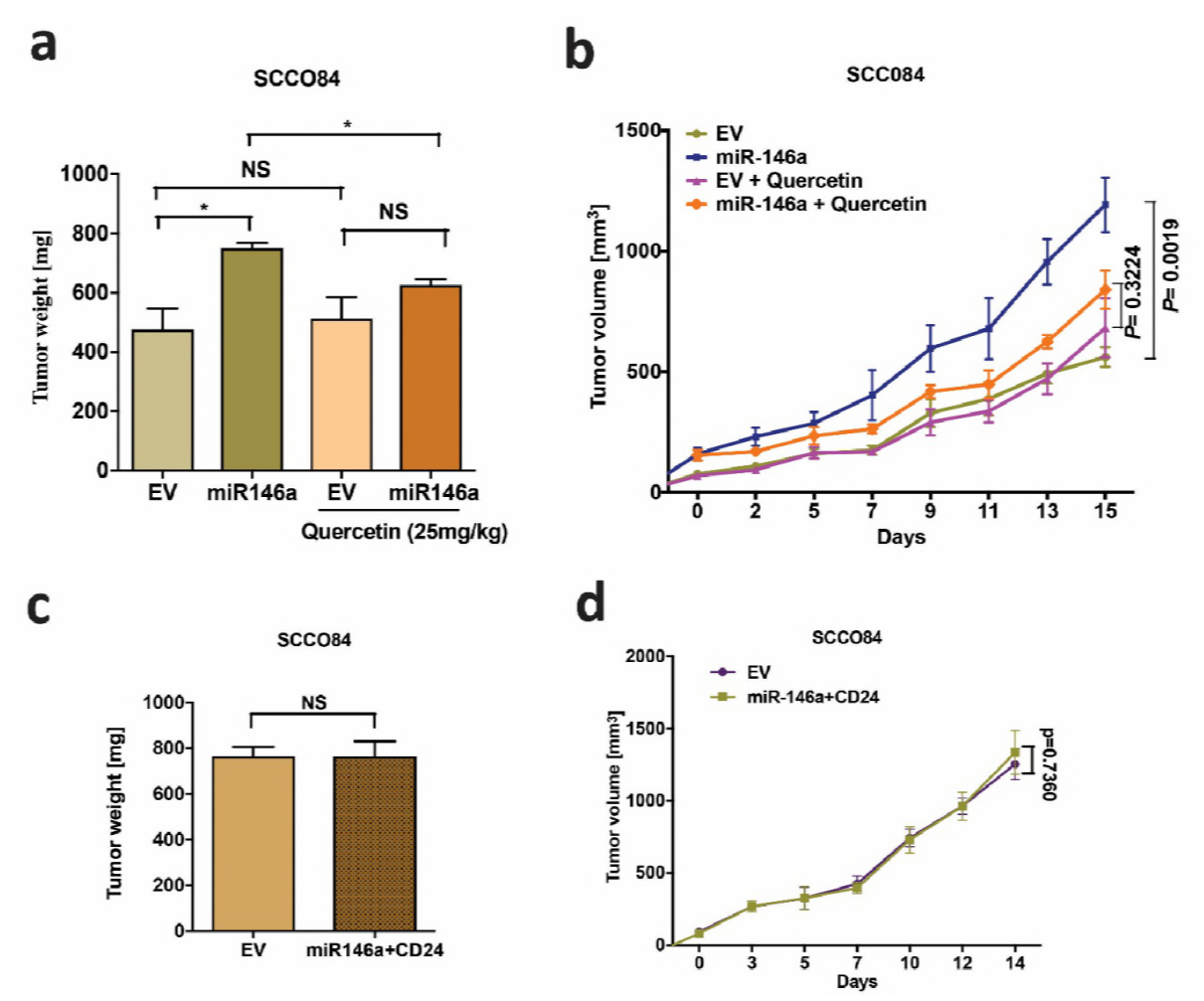

Figure 7

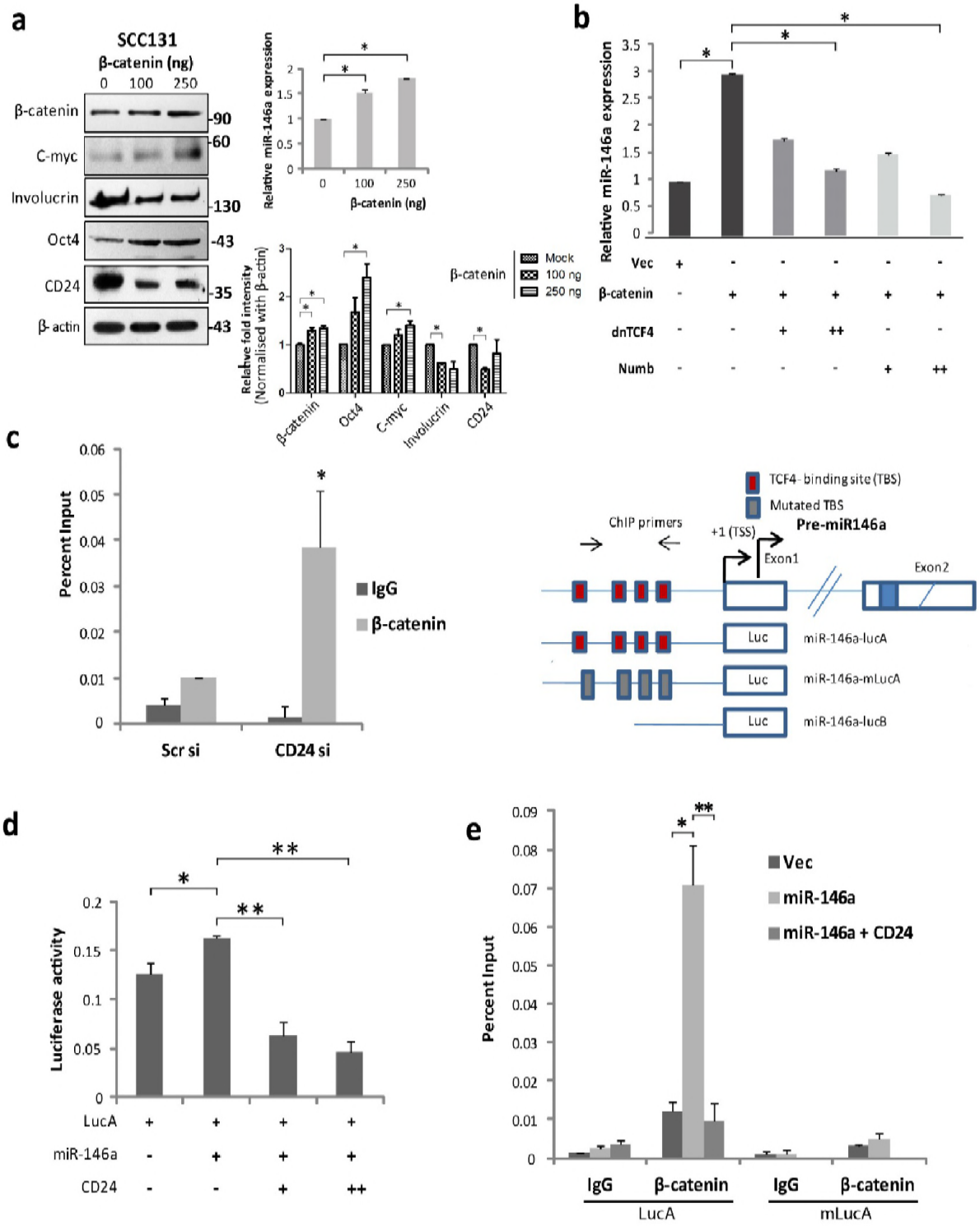

802

803

804 **Figure 8**

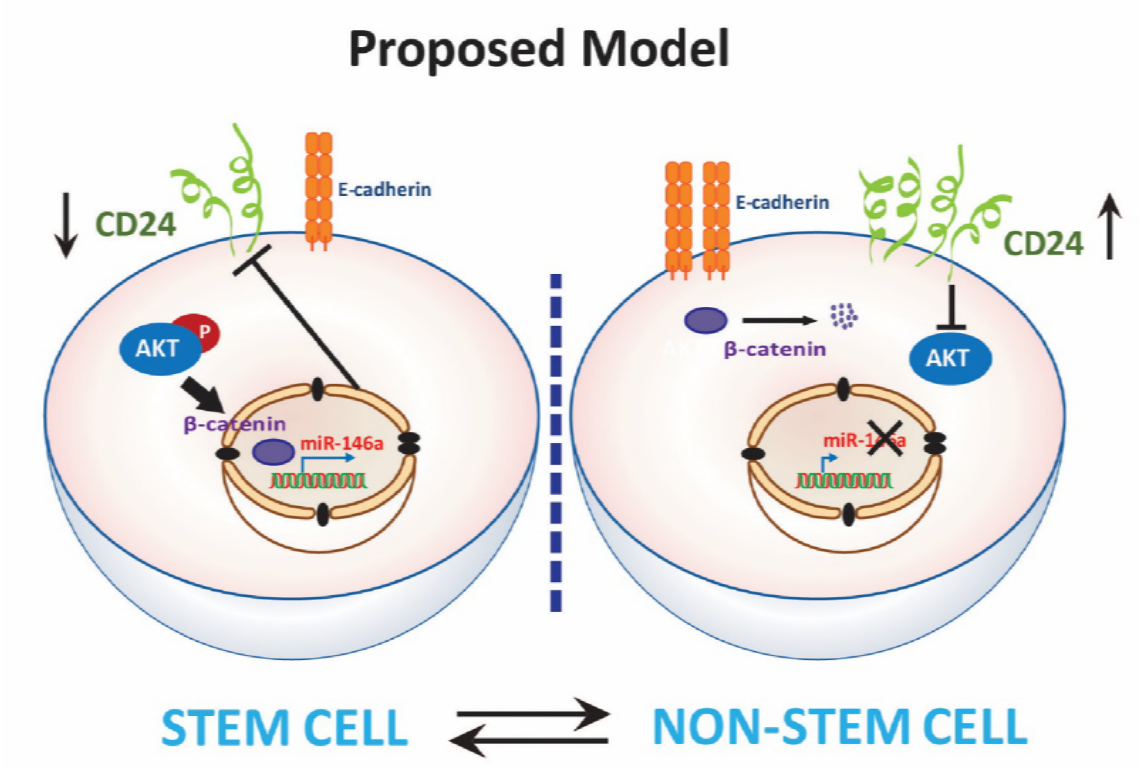

805

806

807

Node Postive group

bcr_patient_barcode	hsa-miR-146a
TCGA-BA-4077	203.493174
TCGA-F7-A61V	#N/A
TCGA-C9-A47Z	39.004298
TCGA-F7-A624	#N/A
TCGA-IQ-A61K	#N/A
TCGA-BA-A6DF	#N/A
TCGA-IQ-A61G	#N/A
TCGA-IQ-A61J	#N/A
TCGA-KU-A66S	#N/A
TCGA-BA-A6DA	#N/A
TCGA-BA-6870	536.192164
TCGA-CV-6951	77.749028
TCGA-CR-6481	540.841402
TCGA-BA-6871	93.860077
TCGA-CR-6473	909.354573
TCGA-BA-6873	101.434427
TCGA-CR-6474	129.58015
TCGA-CR-6482	513.891735
TCGA-BA-A6D8	#N/A
TCGA-CN-5363	223.028852
TCGA-CN-4731	105.945211
TCGA-CV-5441	303.681574
TCGA-CV-5440	105.071181
TCGA-CV-5436	183.723601
TCGA-CV-5431	423.784951
TCGA-CV-6936	149.315762
TCGA-CV-6945	120.656133
TCGA-CR-6491	89.428559
TCGA-CR-6477	323.605516
TCGA-CN-4730	231.329511
TCGA-CV-7248	174.008538
TCGA-CV-6956	211.126418
TCGA-CV-7102	170.426376
TCGA-CV-7424	111.937204
TCGA-CR-7377	324.671929
TCGA-CR-7399	372.056084
TCGA-CR-7388	223.758199
TCGA-BA-7269	56.136435
TCGA-CV-7422	252.031164
TCGA-CR-5247	45.164883
TCGA-CR-7373	191.941966
TCGA-F7-A50I	#N/A
TCGA-CQ-5334	93.212831
TCGA-F7-A61W	#N/A

TCGA-CN-6016	70.569359
TCGA-CV-5442	107.09756
TCGA-CV-5443	211.000154
TCGA-CV-7435	146.280523
TCGA-CN-6989	190.979772
TCGA-CR-6478	573.891756
TCGA-CN-5364	386.388399
TCGA-CN-6998	115.201778
TCGA-CR-7379	73.279815
TCGA-CN-6022	128.226238
TCGA-F7-A620	#N/A
TCGA-CN-6013	193.785719
TCGA-CV-5434	191.952242
TCGA-CN-6018	292.367967
TCGA-DQ-7589	128.668831
TCGA-DQ-7594	165.354955
TCGA-CV-7236	238.921865
TCGA-DQ-7591	839.510595
TCGA-CR-7385	1120.533954
TCGA-CV-5430	226.676337
TCGA-CN-6024	49.551375
TCGA-CR-7404	304.087047
TCGA-CV-6934	278.502098
TCGA-CV-6959	256.715911
TCGA-CN-6996	258.186615
TCGA-CV-6939	552.672435
TCGA-CN-6994	63.62663
TCGA-CN-4726	75.420806
TCGA-BA-4075	#N/A
TCGA-BA-5559	376.808761
TCGA-BA-5555	240.042868
TCGA-CN-5358	294.219965
TCGA-CR-5243	262.477422
TCGA-CV-7433	163.202901
TCGA-BA-6868	74.289075
TCGA-CV-6950	52.434178
TCGA-CV-7104	111.208536
TCGA-CN-6997	102.168699
TCGA-HD-7754	67.573428
TCGA-CV-7095	125.561698
TCGA-CN-6020	282.532532
TCGA-DQ-7593	388.586824
TCGA-DQ-7596	256.152245
TCGA-CR-7397	131.345957
TCGA-CR-7392	360.852101
TCGA-CX-7219	131.0043
TCGA-CV-7414	26.379063

TCGA-CV-7263	201.559848
TCGA-CQ-5329	103.153356
TCGA-CQ-5330	82.341952
TCGA-CQ-5327	198.924526
TCGA-BA-A6DD	#N/A
TCGA-CV-7409	147.109817
TCGA-CR-6492	407.41425
TCGA-CN-6995	339.588177
TCGA-F7-A50J	#N/A
TCGA-CN-6012	218.415148
TCGA-CQ-5324	118.360922
TCGA-CN-6017	259.263506
TCGA-DQ-7590	609.338217
TCGA-CR-7394	389.069099
TCGA-CR-5248	520.348241
TCGA-DQ-7588	191.764336
TCGA-DQ-7592	161.320441
TCGA-CX-7086	176.867346
TCGA-F7-A623	#N/A
TCGA-HD-8314	125.008935
TCGA-CQ-5326	77.455924
TCGA-CR-6467	324.705845
TCGA-CR-6472	75.258578
TCGA-BA-5557	171.714349
TCGA-BA-5558	182.472549
TCGA-CV-7428	174.254658
TCGA-CR-7382	253.892599
TCGA-CV-7432	235.535454
TCGA-CV-6954	145.16574
TCGA-CN-6988	83.344871
TCGA-CN-6992	77.124382
TCGA-CR-6470	284.554637
TCGA-CR-6493	43.006432
TCGA-BA-6872	122.674568
TCGA-CR-6480	343.005882
TCGA-BA-4074	144.585941
TCGA-CN-5361	340.999352
TCGA-CN-5359	368.09132
TCGA-CN-5374	517.080741
TCGA-BA-4078	100.172146
TCGA-CN-5365	145.268883
TCGA-CN-4728	469.774224
TCGA-MT-A51W	#N/A
TCGA-MT-A51X	#N/A
TCGA-BA-4076	98.044129
TCGA-CN-5366	136.155245
TCGA-CN-5369	312.628619

TCGA-HD-A4C1	73.94964
TCGA-CN-A49B	211.578519
TCGA-D6-6826	120.656921
TCGA-CQ-6229	315.341462
TCGA-CQ-6227	87.289259
TCGA-CQ-6220	219.303627
TCGA-CQ-6219	500.901142
TCGA-D6-6824	222.9591
TCGA-CQ-6222	461.48393
TCGA-CQ-6228	55.330093
TCGA-D6-6827	1354.108337
TCGA-D6-6823	160.681401
TCGA-DQ-5631	170.311568
TCGA-DQ-5629	104.852923
TCGA-DQ-5624	137.770464
TCGA-DQ-5630	100.825603
TCGA-D6-6516	104.347384
TCGA-BB-4227	23.943223
TCGA-CN-4742	162.452586
TCGA-BA-5149	207.508447
TCGA-D6-A4Z9	162.365488
TCGA-HD-7229	182.70726
TCGA-CV-7178	481.805615
TCGA-CV-7089	177.357782
TCGA-CR-7389	155.282503
TCGA-CR-7386	175.181465
TCGA-CR-7367	143.122516
TCGA-CR-7365	85.694878
TCGA-BB-4217	307.532593
TCGA-CV-5977	96.056128
TCGA-CV-5979	37.963951
TCGA-CV-5978	235.268394
TCGA-CV-5976	155.632227
TCGA-CV-5971	275.748969
TCGA-CV-5966	171.903942
TCGA-CV-5970	88.495487
TCGA-CQ-7064	81.985763
TCGA-H7-8502	54.46137
TCGA-BB-8596	110.118089
TCGA-HD-8635	232.678718
TCGA-CQ-7063	125.122997
TCGA-HD-8634	204.545066
TCGA-H7-8501	207.416135
TCGA-HD-7832	153.766972
TCGA-F7-7848	164.556141
TCGA-CN-4735	683.869429
TCGA-BB-4225	269.958215

TCGA-BB-4223	452.573877
TCGA-BA-5153	543.966271
TCGA-BB-7871	146.933594
TCGA-BB-7870	131.128002
TCGA-BB-7866	323.792934
TCGA-BB-7862	100.295919
TCGA-BB-7864	71.003387
TCGA-HL-7533	116.653572
TCGA-BB-7872	275.052401
TCGA-BB-7861	559.710537
TCGA-P3-A5Q5	#N/A
TCGA-P3-A5QF	#N/A
TCGA-P3-A5QE	#N/A

Node Negative group

bcr_patient_barcode	hsa-miR-146a
TCGA-F7-8298	72.925749
TCGA-CV-6436	117.884732
TCGA-CV-6938	317.433805
TCGA-C9-A480	136.919867
TCGA-BA-A6DB	#N/A
TCGA-IQ-A61H	#N/A
TCGA-IQ-A61E	#N/A
TCGA-CR-6471	188.583433
TCGA-CN-5373	146.914012
TCGA-CN-5360	362.49953
TCGA-CV-5444	212.584384
TCGA-CR-5249	800.740572
TCGA-CV-7438	280.295951
TCGA-CR-7383	186.816823
TCGA-CV-6952	183.219357
TCGA-CV-6940	109.527988
TCGA-CQ-5333	296.916468
TCGA-CR-7370	57.692743
TCGA-CV-6962	118.630688
TCGA-CV-6943	195.741626
TCGA-CN-5355	113.137321
TCGA-CN-4729	476.947392
TCGA-CN-5367	235.090603
TCGA-CN-5356	212.673093
TCGA-CV-7097	241.595567
TCGA-CV-7101	236.650996
TCGA-CV-7238	282.182157
TCGA-CV-7425	555.121507
TCGA-CV-7427	255.324226
TCGA-CV-7416	150.779146
TCGA-CV-7415	114.973413
TCGA-CV-7253	37.96632
TCGA-CV-6960	160.119126
TCGA-CX-7085	198.492307
TCGA-CV-5435	42.148361
TCGA-CN-6023	263.892477
TCGA-CN-6021	142.610915
TCGA-CV-7568	66.701619
TCGA-CV-7429	95.602569
TCGA-CV-6941	101.892332
TCGA-CN-4722	202.478143
TCGA-CV-7254	1202.264843
TCGA-CR-7395	232.803306
TCGA-CV-5439	260.049518

TCGA-CV-7235	889.589848
TCGA-CR-7372	85.792484
TCGA-CV-7255	416.946383
TCGA-CV-7418	80.751546
TCGA-CR-7401	140.400497
TCGA-CN-5370	110.91965
TCGA-CV-7407	215.522849
TCGA-CV-7421	85.176783
TCGA-CR-7374	219.574573
TCGA-CQ-5325	386.721341
TCGA-D6-8568	152.880938
TCGA-BB-8601	35.516371
TCGA-HD-8224	33.297366
TCGA-CV-7430	57.104797
TCGA-CV-6953	190.973833
TCGA-CV-6961	35.435729
TCGA-CR-6484	158.68964
TCGA-BA-6869	322.264183
TCGA-BA-5556	396.390766
TCGA-CR-5250	328.525344
TCGA-CR-7376	219.696468
TCGA-CV-7446	47.687344
TCGA-CV-6933	328.370206
TCGA-CR-7390	140.88121
TCGA-CR-7398	112.521326
TCGA-CR-7391	341.018343
TCGA-CV-7250	138.642893
TCGA-CV-7410	273.928134
TCGA-CV-7247	121.240789
TCGA-CV-7413	131.5283
TCGA-CV-7252	112.342497
TCGA-CN-6019	619.959064
TCGA-CQ-5323	216.189978
TCGA-CN-6011	115.577523
TCGA-CV-7099	380.835863
TCGA-CR-7380	128.778186
TCGA-CV-7245	112.376736
TCGA-CR-6488	136.598963
TCGA-IQ-7632	168.748174
TCGA-CV-6942	353.920916
TCGA-CR-7402	246.567762
TCGA-CX-7082	220.377078
TCGA-HD-7753	150.988219
TCGA-CV-7411	168.929143
TCGA-IQ-7630	237.985446
TCGA-CV-7261	156.769613
TCGA-CV-7091	120.199014

TCGA-CQ-5332	70.877908
TCGA-CV-5432	129.103043
TCGA-CV-6433	623.938945
TCGA-D6-8569	199.931452
TCGA-DQ-7595	185.763779
TCGA-CV-7103	182.321386
TCGA-CR-7393	307.374351
TCGA-CV-6937	149.402772
TCGA-CV-7242	271.309959
TCGA-CV-7406	103.415984
TCGA-IQ-7631	9.426839
TCGA-CV-6955	298.004749
TCGA-CV-7100	78.019919
TCGA-CV-7090	270.239157
TCGA-CV-6003	114.365252
TCGA-CN-6010	142.711713
TCGA-CR-7371	226.861626
TCGA-CV-7423	134.348989
TCGA-CV-7243	69.258781
TCGA-CV-6441	159.532248
TCGA-BA-A6DE	#N/A
TCGA-F7-8489	220.312975
TCGA-CR-6487	327.350047
TCGA-CV-7440	169.713168
TCGA-CV-7437	240.395329
TCGA-CV-7434	339.201541
TCGA-CV-6935	110.994004
TCGA-CV-6948	88.064455
TCGA-CQ-5331	351.738909
TCGA-CN-4723	310.504995
TCGA-CN-4725	89.807373
TCGA-CN-4727	242.466603
TCGA-CQ-6225	57.80891
TCGA-CQ-6223	166.688126
TCGA-CQ-6218	161.104923
TCGA-D6-6825	247.021917
TCGA-CQ-6224	69.350806
TCGA-BA-5152	631.609232
TCGA-DQ-5625	106.458022
TCGA-D6-6517	220.940955
TCGA-D6-6515	317.356789
TCGA-CN-4733	289.702104
TCGA-CN-4738	254.287346
TCGA-CN-4739	434.852353
TCGA-D6-A4ZB	186.485982
TCGA-CR-7364	116.255161
TCGA-CV-7183	87.069539

TCGA-CV-7177	112.674656
TCGA-CV-7180	182.869117
TCGA-H7-7774	295.608723
TCGA-CQ-7068	181.791608
TCGA-CQ-6221	480.55317
TCGA-CQ-7065	23.8474
TCGA-CV-5973	24.400472
TCGA-CQ-7069	27.764594
TCGA-HD-7831	95.771431
TCGA-CR-7369	143.038792
TCGA-CR-7368	213.989357
TCGA-CN-4734	#N/A
TCGA-CN-4737	79.848209
TCGA-CN-4736	326.181646
TCGA-BB-4228	110.911183
TCGA-CN-4741	415.204395
TCGA-CN-4740	223.561348
TCGA-BB-4224	53.407918
TCGA-BA-5151	188.891666
TCGA-HD-7917	101.231353
TCGA-CQ-7067	86.701001
TCGA-BB-7863	83.382842
TCGA-P3-A5QA	#N/A
TCGA-P3-A5Q6	#N/A

ChIP Primers

Endogeneous miR-146a promoter

146A_P2_F:	CCCAAGTAGCTGGGACTACA
146A_P2_R:	TAGGCGAGATGTGGTGACTC

Luciferase miR-146a promoter

TBS-chip_F	CTTGAATGTTCACATTTCCAGAG
TBS-chip_R	GGCAGAAAGCTCCCTTGTTTC